

铀同位素研究进展及其在 铀矿床中的应用

抄尉尉^{1, 2)}, 姚东东²⁾, 冷成彪^{1, 2)}, 王大钊^{1, 2)}, 王艳军^{1, 2)},
田世洪^{1, 2)}, 梁正伟^{1, 2)}, 程强龙²⁾

1) 东华理工大学铀资源探采与核遥感全国重点实验室, 南昌, 330013

2) 东华理工大学地球与行星科学学院, 南昌, 330013

内容提要: 铀作为自然界中重要的放射性元素, 其同位素分馏行为在铀矿成因研究、地球化学过程示踪及环境修复方面具有重要应用价值。本文系统综述了铀同位素的分馏机理(核体积效应、氧化还原、吸附与淋滤过程)、高精度测试方法(化学前处理与质谱分析技术)和全球主要储库(大陆地壳、地幔、海洋系统等)的铀同位素组成特征, 及其在砂岩型、花岗岩型等典型铀矿床研究中的应用进展。文章指出, 铀同位素在识别成矿环境、示矿物物质来源、揭示氧化还原过程等方面具有独特优势, 并对其在深部地球过程、成矿机制和矿山修复监测等领域的未来研究方向进行了展望, 为深化铀矿床成因理论与资源勘查提供了重要参考。

关键词: 铀同位素; 同位素分馏; 核体积效应; 铀矿床; 氧化还原过程

铀作为主要的放射性元素之一, 其天然同位素包括²³⁸U (99.2742%)、²³⁵U (0.7024%) 和²³⁴U (0.0054%) (Meija et al., 2016) (图1)。²³⁸U 和²³⁵U 最终分别衰变为稳定同位素²⁰⁶Pb 和²⁰⁷Pb, 半衰期分别为4468 Ma 和703.8 Ma (Jaffey et al., 1971)。这一衰变体系构成了 U-Pb 同位素定年的理论基础, 是地球科学研究的重要支柱(骆金诚等, 2019)。在地球4.56 Ga 的漫长演化过程中, 由于半衰期差异, ²³⁸U/²³⁵U 比值已从初始值3.3 升高至现在的约137.88。该比值曾长期被视为恒定, 但近年研究发现, 以标准物质 CRM-145 为基准进行标准化后, $\delta^{238}\text{U}$ (即²³⁸U/²³⁵U 的相对偏差) 存在显著变化 (Weyer et al., 2008; Voinot et al., 2024), 其主要原因是氧化还原过程中产生了核体积效应 (Bigeleisen, 1996; Weyer et al., 2008; Tissot and Dauphas, 2015; Andersen et al., 2017; Li Haoyu and Tissot, 2023)。随着测试精度的不断提高(相对误差<0.1‰), 铀同位素在高温至低温地球化学过程中的应用日益广泛 (Hiess et al., 2012; Tissot and Dauphas, 2015; Andersen et al., 2017; Tissot and

Ibañez-Mejía, 2021; 梁正伟和田世洪, 2021; 宋静等, 2022)。近年来铀同位素研究进一步拓展至岩浆作用及相关过程, 涵盖结晶分异、热扩散、地幔交代、俯冲过程、沉积再循环以及蛇纹岩风化作用等多个方面 (Telus et al., 2012; Andersen et al., 2015; Tissot et al., 2017; Freymuth et al., 2019; Li Haoyu and Tissot, 2023; Pavia et al., 2023)。在自然界中, 铀主要以 U⁴⁺ 和 U⁶⁺ 两种氧化态存在 (Langmuir, 1978)。U⁴⁺ 溶解度极低, 通常以 UO₂ 形式稳定存在, 是地幔中铀的主要赋存状态 (Wood et al., 1999); U⁶⁺ 具有高度溶解性与强迁移能力, 在水体中可形成多种水合及配合物形态, 如 UO₂²⁺、UO₂(OH)_{2(aq)} 和 UO₂(OH)₃⁻ 等, 其中碳酸铀酰络合物是其主要的存在形式 (Langmuir, 1978; 王大钊等, 2022)。

铀矿床在地球历史上多个时期均可形成, 其成因不仅与大型盆地演化紧密相关 (陈振宇等, 2014; 胡瑞忠等, 2019; 张龙等, 2021; 张明林等, 2025), 也与重大氧化事件直接关联 (Partin et al., 2013; 李子颖等, 2021; Voinot et al., 2024)。鉴于铀资源



注: 本文为国家自然科学基金资助项目(编号:42473044), 铀资源探采与核遥感全国重点实验室(东华理工大学)自主部署基金资助项目(编号:2025QZ-YZZ-07 和 2025QZ-KF-04)和江西省自然科学基金资助项目(编号:20252BAC200255 和 20252BAC220018)的成果。

收稿日期:2025-11-13; 改回日期:2026-02-02; 网络首发:2026-02-15; 责任编辑:章雨旭。Doi: 10.16509/j.georeview.2026.02.045

作者简介:抄尉尉,男,1991年生,副研究员,主要从事热液矿床研究;Email: chaoweimei@ecut.edu.cn。通讯作者:冷成彪,男,1982年生,教授,长期从事矿床学与地球化学方面的教学与研究工作;Email: leb8207@163.com。

的战略重要性,目前已有十余类铀矿床采用铀同位素方法开展研究(Bopp et al., 2009; Brennecke et al., 2010; Murphy et al., 2014; Uvarova et al., 2014; Kirchenbaur et al., 2016; Keatley et al., 2021)。对于铀这类重元素,其同位素在氧化还原反应等化学反应过程中会发生非质量分馏,这主要源于原子核正电荷分布与核形态的差异,即核体积效应(Schauble, 2007)。在此机制下,较重的同位素倾向于富集在电子密度最低的化学物种中(Bigeleisen, 1996)。对铀而言,还原态物种的原子核电子密度最低(Bigeleisen, 1996),因此较重的铀同位素(^{238}U)通常富集于还原态固相中(Weyer et al., 2008; Uvarova et al., 2014)。自然体系氧化还原条件的准确识别,对于理解成矿机制、处理矿井水与尾矿、评估核废料处置库长期稳定性等方面具有关键意义(Robert and Lovley, 2002; Stirling et al., 2007; Uvarova et al., 2014)。其中,铀矿床研究尤为关键且具挑战性:一方面,许多铀矿床形成后,构造活动仍在持续(Dieng et al., 2013, 2015);另一方面,此类环境中常存在氧化还原状态迥异的流体相互作用(Uvarova et al., 2014; Voinot et al., 2024)。

随着高精度质谱分析技术的突破性发展,由核体积效应主导的铀同位素(特别是 $^{238}\text{U}/^{235}\text{U}$)非质量分馏,已被证实是揭示地球化学过程中氧化还原状态和反应机制的强大示踪工具。本文旨在对铀同位素地球化学的研究现状进行一次全面而系统的梳理和整合,深入阐释其在铀矿床成因研究、资源勘探及环境评估中的关键作用和广阔前景,为相关学者提

供参考。

1 铀同位素分馏机理

早期研究发现铀矿石中 $^{238}\text{U}/^{235}\text{U}$ 比值的变化幅度极小,不超过0.1%(Cowan and Adler, 1976)。随后学界提出,整个太阳系(含地球) $^{238}\text{U}/^{235}\text{U}$ 推荐值为137.88(Steiger and Jäger, 1977)。进入21世纪以后,随着双稀释剂方法与高精度分析技术的开发和应用,铀同位素分析精度显著提升,研究人员发现了除衰变过程外的铀同位素分馏现象(Rademacher et al., 2006; Stirling et al., 2007; Weyer et al., 2008; Goldmann et al., 2015)。以下对主要的同位素分馏机理进行总结。

1.1 核体积效应

核体积效应(亦称核场位移效应, Nuclear field shift effects, NFSE)是指由原子核尺寸与形状的差异引起基态电子能变化,进而引发同位素分馏的现象(Gagné et al., 1976, 1977, 1978; Schauble, 2007; Knyazev and Myasoedov, 2001; Yang Sha and Liu Yun, 2016)(图2)。

该效应最早由Fujii et al. (1989a, b)在 $\text{U}^{4+}-\text{U}^{6+}$ 交换反应中发现:他们观察到奇数质量数同位素 ^{235}U 的分馏因子与相邻偶数质量数同位素之间不成线性关系,形成典型的奇偶交错分布模式。随后, Nishizawa et al. (1994, 1995)与 Nomura et al. (1996)将 ^{87}Sr 和 ^{233}U 的异常分馏归因于此效应。Bigeleisen(1996, 1998)首次将核体积效应系统引入

同位素分馏的理论计算框架,指出仅通过基态电子能的变化即可引起显著的同位素分馏。Schauble(2007)率先基于量子化学方法计算了Hg、Tl等重金属同位素的分馏系数;此后, Schauble(2013)与 Fang Tong and Liu Yun(2019)进一步发展了适用于固相体系的核体积效应计算方法。根据杨莎和刘耘(2015),核体积效应在同位素交换反应中的表达式为:

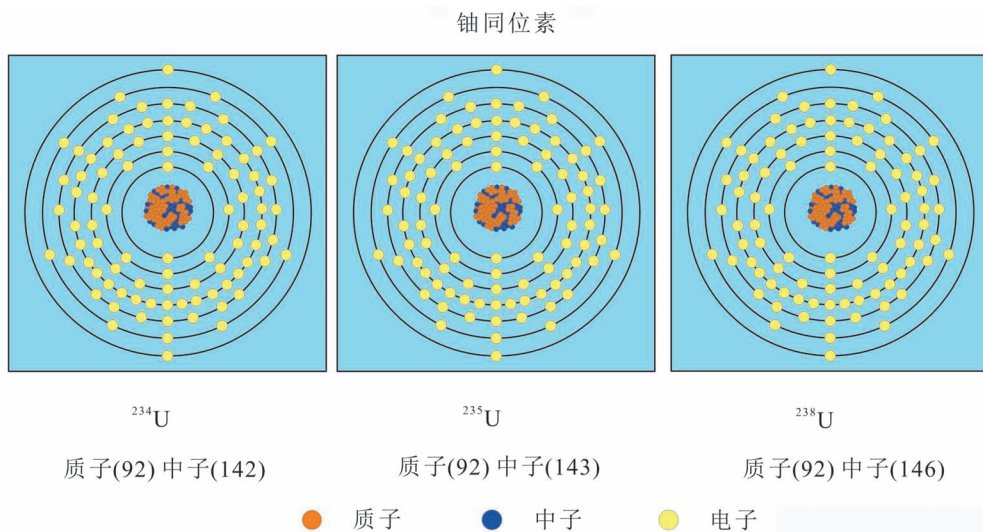


图1 铀的三种天然同位素

Fig. 1 The three naturally occurring isotopes of uranium

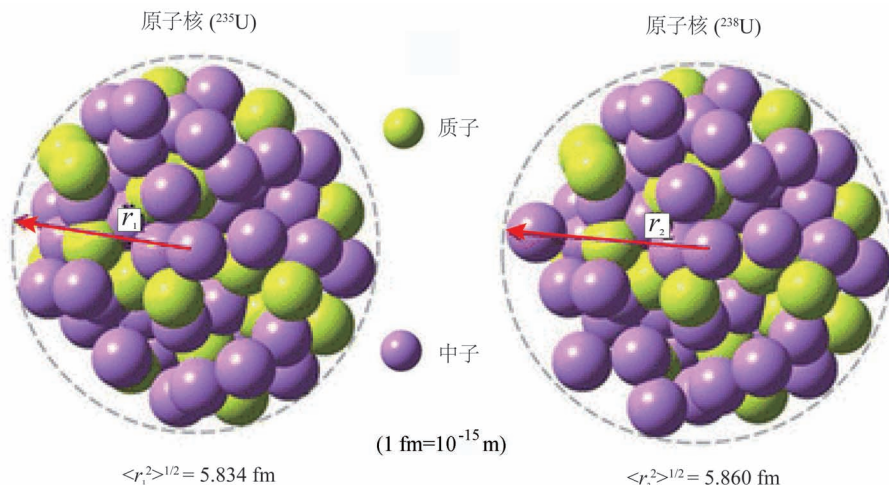


图2 具有有限核尺寸的铀同位素原子核

Fig. 2 Uranium isotope nuclei with finite nuclear sizes

中子数的差异会导致同位素的核尺寸与形状不同(即核半径 r_1 和 r_2 存在差异),例如 ^{235}U

和 ^{238}U 的均方根核电荷半径分别为5.834 fm和5.860 fm($1 \text{ fm} = 10^{-15} \text{ m}$)

Differences in the number of neutrons cause variations in the nuclear sizes and shapes of isotopes (i. e., differences in nuclear radius r_1 and r_2). For example, the root mean-square charge radii of ^{235}U and ^{238}U are 5.834 femtometers and 5.860 femtometers, respectively

$$\ln K_{fs} =$$

$$\frac{[E_0(\text{AX}) - E_0(\text{A}'\text{X})] - [E_0(\text{AY}) - E_0(\text{A}'\text{Y})]}{kT}$$

其中, $\ln K_{fs}$ 是核体积效应引起的平衡常数; E_0 为基态电子能;AX和A'X、AY和A'Y分别为不同同位素取代的化合物; k 为波尔兹曼常数($1.380649 \times 10^{-23} \text{ J/K}$); T 是绝对温度(K)。在恒定温度下,电子能的变化与核电子密度差及同位素核半径均方差成正比:

$$\delta E_{fs} \propto [|\psi(0)_A|^2 - |\psi(0)_B|^2] \cdot \delta \langle r^2 \rangle_{ij}$$

式中, δE_{fs} 为电子能变化, $[|\psi(0)|]^2$ 表示电子在原子核处的概率密度, $\delta \langle r^2 \rangle_{ij}$ 为同位素核半径的均方差。

上述理论表明,核体积效应导致重铀同位素(如 ^{238}U)倾向于在还原态物质中富集(Shimokawa and Kobayashi, 1970; Florence et al., 1975; Fujii et al., 1989a, b, 2006; Nakanishi et al., 1996),该结论与基于振动质量效应的传统质量分馏模型的预测结果相反(图3)。值得注意的是,质量相关分馏的幅度与 $1/T^2$ 成正比,随温度升高快速减弱;而核体积效应与 $1/T$ 成正比,随温度升高而衰减缓慢。因此,在高温环境(如火山岩形成过程)中,核体积效应对总同位素分馏的相对贡献将更为显著(Tissot

and Ibañez-Mejia, 2021)。需要强调的是,核体积效应本质上是平衡效应;其驱动同位素分馏的关键并非铀的还原反应本身,而是不同价态铀之间建立的化学平衡,该平衡为核体积效应的出现提供了必要条件(Andersen et al., 2017)。

1.2 氧化还原过程

当前针对铀同位素分馏的研究主要围绕 U^{6+} 的还原反应体系展开,该过程可分为生物还原与非生物还原两大类(Rademacher et al., 2006; Stirling et al., 2007; Basu et al., 2014; Stirling et al., 2015; Stylo et al., 2015b)。生物还原主要依赖金属还原菌和硫酸盐还原菌等微生物实现(Rademacher et al.,

2006; Basu et al., 2014; Stirling et al., 2015; Stylo et al., 2015a; Basu et al., 2020; Dang et al., 2022),而非生物还原过程则利用零价金属、 Fe^{2+} 、硫化物及还原性有机质等作为还原介质(Rademacher et al., 2006; Stirling et al., 2007; Stylo et al., 2015b; Brown et al., 2018)。在生物还原作用过程中,微生物会优先摄取 ^{238}U 并将其转移至还原相,导致残余 U^{6+} 库中 $\delta^{238}\text{U}$ 值下降约1‰(Basu et al., 2014; Stirling et al., 2015; Stylo et al., 2015a, b; Basu et al., 2020)。相比之下,使用零价金属(如 Fe^0 , Rademacher et al., 2006; Zn^0 , Stirling et al., 2007)或有机质(如泥炭, Stylo et al., 2015b)进行的非生物还原实验中,未检测到明显的铀同位素分馏;而多数以 Fe^{2+} 或硫化物为还原剂的非生物体系虽可产生可分辨的分馏,但其方向却与生物还原相反,表现为 ^{238}U 在残余 U^{6+} 库中富集(Stylo et al., 2015b)。这些结果曾被归纳为“仅生物还原才能引发显著的核体积效应”。然而,Brown et al. (2018)的研究表明,在特定非生物还原过程(起始铀浓度较低、 HCO_3^- 含量和pH值较高)中, ^{238}U 可能同样优先进入还原态含铀相。该研究进一步揭示, $^{238}\text{U}/^{235}\text{U}$ 分馏本质上是平衡同位素分馏(核体积效应)与动力学同位素分馏共同作用的结果(图

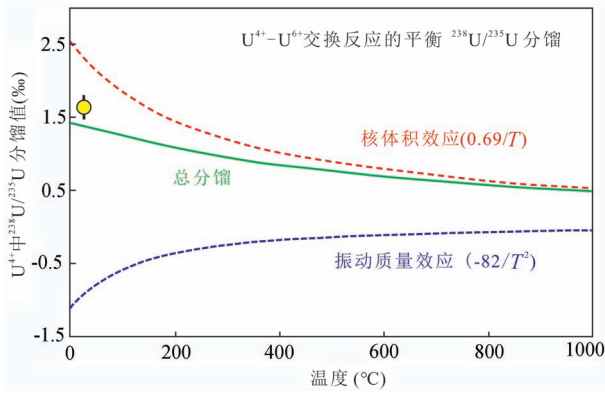


图3 基于氯化物介质 $U^{6+}-U^{4+}$ 交换平衡态同位素分馏实验数据绘制的温度与 $^{238}U/^{235}U$ 分馏理论趋势图 (修改自 Andersen et al., 2017)

Fig. 3 The theoretical trend diagram of temperature vs. $^{238}U/^{235}U$ fractionation, plotted based on experimental data of uranium isotope fractionation at equilibrium during $U^{6+}-U^{4+}$ exchange in a chloride medium (modified from Andersen et al., 2017)

U^{4+} 中 $^{238}U/^{235}U$ 分馏值 (‰) 指的是 U^{4+} 中 $^{238}U/^{235}U$ 相对于 U^{6+} 中该比值的偏离程度, 实测的 $^{238}U/^{235}U$ 总分馏值由核体效应与质量依赖效应耦合作用。这两种效应对铀同位素的分馏作用方向相反, 且温度依赖性各异, 其中核体效应主导总分馏信号。图示温度区间内对铀同位素分馏影响的估算是基于较窄温度范围 (87 - 160°C) 的实验数据外推得出, 在该范围之外可能产生较大不确定性 (Fujii et al., 2006)。然而, 这些数据与 Wang Xiangli 等 (2015) 在 25°C 条件下获得的实验数据 (圆圈标示) 高度吻合

The isotope fractionation value of $^{238}U/^{235}U$ in U^{4+} (‰) refers to the degree of deviation of the $^{238}U/^{235}U$ in U^{4+} relative to that in U^{6+} . The observed total $^{238}U/^{235}U$ fractionation results from the combined effects of the nuclear volume effect and the mass-dependent effect. These two effects fractionate uranium isotopes in opposing directions and differ in their temperature dependence, with the nuclear volume effect dominating the total fractionation signal. The estimated influence on uranium isotope fractionation within the illustrated temperature range was extrapolated from experimental data obtained over a relatively narrow temperature range (87 - 160 °C), which may introduce significant uncertainties beyond this interval (Fujii et al., 2006). Nevertheless, these data show excellent agreement with experimental results from Wang Xiangli et al. (2015) obtained at 25 °C (indicated by the circle)

4; Brown et al., 2018)。具体而言, 当铀从溶液中快速去除时, 分馏主要由动力学 (质量依赖) 效应主导, 较轻的 ^{235}U 会优先进入还原相沉淀; 而在铀去除速率较慢、 $U^{6+}-U^{4+}$ 体系达到充分同位素平衡的条件下, 核体效应才会完全显现, 导致 ^{238}U 在还原相中富集。相较于还原过程, 铀在氧化过程中的同位

素分馏研究仍较为有限。Wang Xiangli et al. (2015) 通过溶解氧对 U^{4+} 进行氧化的实验发现, 残余还原相中 ^{238}U 的富集程度极低, 推测可能是“皮层效应”限制了显著分馏的发生; 即固态 U^{4+} 的表层必须被完全氧化后, 下一层才能暴露于氧化剂, 这种逐层转化导致同位素分馏效应极为微弱。

1.3 吸附过程

除了氧化还原过程, 吸附作用也是引发铀同位素分馏的重要机制。多种矿物 (如水钠锰矿、石英、针铁矿、伊利石、铁锰结壳/结核) 以及微生物均可作为铀的吸附载体 (Greathouse et al., 2002; Catalano and Brown, 2005; Brennecke et al., 2011b; Singh et al., 2012; Acharya and Apte, 2013; Rihs et al., 2014; Fang Tong and Liu Yun, 2019)。矿物表面吸附铀所产生的同位素分馏, 一般认为与溶液中溶解态 U^{6+} 和表面吸附态 U^{6+} 在配位几何结构上的差异有关 (Dang et al., 2016; Jemison et al., 2016) (图 5)。类似地, 微生物通过其表面官能团 (如羟基、羧基、氨基、磷酸基、巯基等) 吸附铀时, 也会引

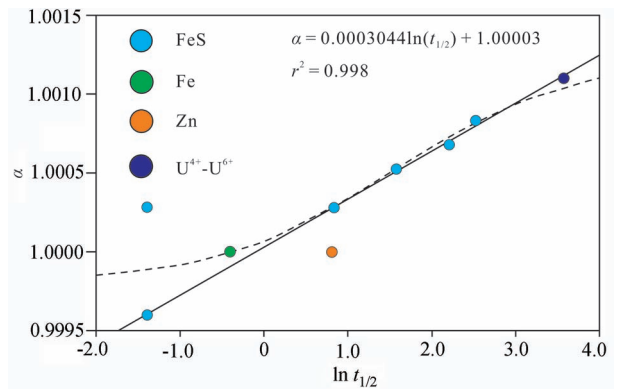


图4 铀在液体中的去除半衰期 ($t_{1/2}$) 与同位素分馏因子 (α) 之间的关系图 (引自 Brown et al., 2018)

Fig. 4 Relationship between the uranium residence time in liquid and the isotopic fractionation factor (modified from Brown et al., 2018)

$t_{1/2}$ 为水溶液中 U^{6+} 浓度降至初始值 50% 所需时间, α 为 $(^{238}U/^{235}U)_{\text{残余水溶液}} / (^{238}U/^{235}U)_{\text{初始水溶液}}$, 不同的圆圈颜色代表不同的还原介质或反应机制, 虚线代表质量依赖分馏模拟曲线

$t_{1/2}$ is the time required for the concentration of U^{6+} in the aqueous solution to decrease to 50% of its initial value. α is defined as $(^{238}U/^{235}U)_{\text{residual aqueous solution}} / (^{238}U/^{235}U)_{\text{initial aqueous solution}}$. The different circle colors denote distinct reducing media or reaction mechanisms, while the dashed line represents the modeled curve for mass-dependent fractionation

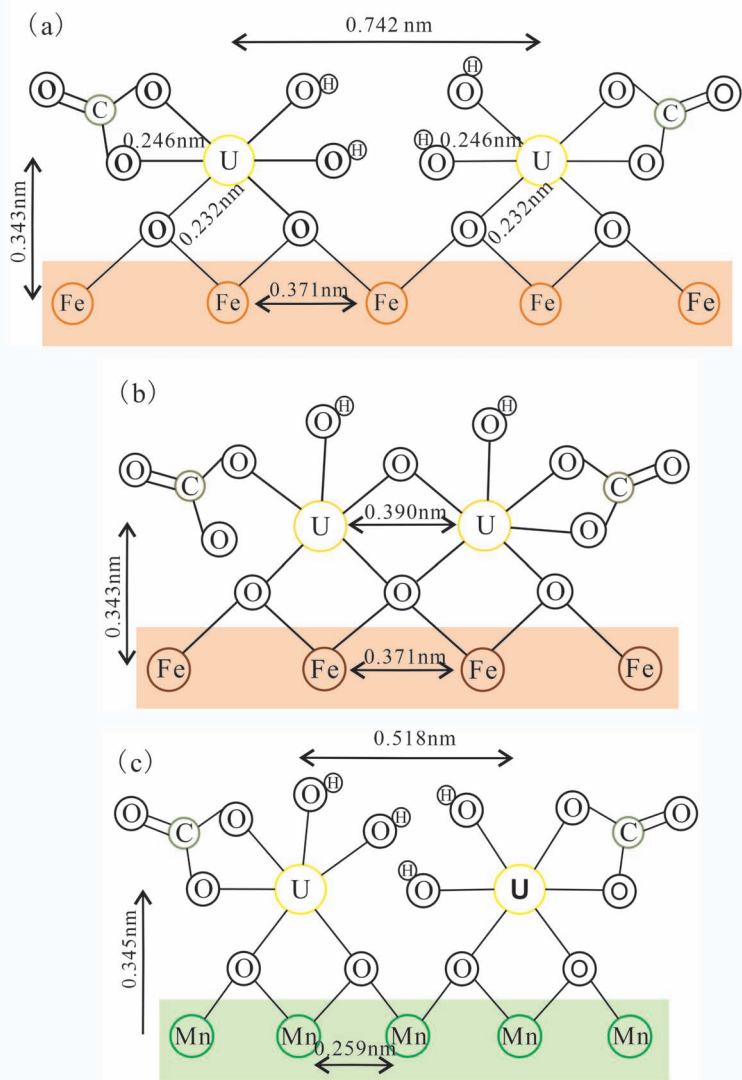


图5 铀在铁锰氧化物表面的吸附模型(修改自 Dang et al., 2016): (a) 铀以单齿配体形式吸附到赤铁矿表面; (b) 铀以双齿配体形式吸附到赤铁矿表面; (c) 铀以单齿配体形式吸附到锰氧化物表面

Fig. 5 Sorption model of uranium on iron—manganese oxide surfaces (modified from Dang et al., 2016): (a) Uranium adsorbed on the hematite surface by bidentate-monodentate binding; (b) uranium adsorbed on the hematite surface by bidentate-binuclear binding; (c) uranium adsorbed on the manganese oxide surface by bidentate-monodentate binding

起溶解态与吸附态 U^{6+} 之间配位环境的改变, 从而驱动同位素分馏 (Acharya et al., 2017)。值得关注的是, 吸附过程导致的铀同位素分馏方向与还原过程相反: 吸附相倾向于富集较轻的同位素 ^{235}U (图5)。例如, 在非还原性吸附过程中, 淡水浮游生物体内富集轻铀同位素, 其与水体之间的分馏值约 0.23‰ (Chen Xinming et al., 2020)。上述吸附实验所观测到的铀同位素分馏方向和范围 (0.15‰~

0.23‰), 与锰结核(壳)和海水之间的分馏范围基本吻合 (Weyer et al., 2008; Goto et al., 2014; Wang Xiangli et al., 2016)。

1.4 淋滤过程

目前, 关于淋滤作用对铀同位素分馏的影响仍不明确。尽管有研究在黑稀金矿和锆石的淋出液中观察到 ^{235}U 的系统性富集 (Stirling et al., 2007; Hiess et al., 2012), 但其他针对锆石和沥青铀矿的研究却发现淋出液与全岩的铀同位素组成并无系统性差异 (Stirling et al., 2007; Livermore et al., 2018)。这种矛盾可能源于两种机制: 其一, 淋滤过程中晶格内弱结合态 ^{235}U 被优先释放; 其二, 淋出液中的氧化态(可溶)铀与矿物中的还原态(不溶)铀之间发生了平衡同位素分馏。要明确淋滤过程对矿物铀同位素组成的具体影响, 仍需开展更多受控实验。与之形成对比的是, 在近地表缺氧环境中, 配体(如碳酸氢盐、铁载体、柠檬酸盐及腐殖质等)可重新活化 U^{4+} , 导致迁移相中 ^{238}U 的富集, 该过程可能与铀在配合物中的键长和键强度变化有关 (Luo Wensui and Gu Baohua, 2011; Prieto et al., 2013; Roebbert et al., 2021)。

2 铀同位素分析方法

2.1 化学前处理

实验所用特氟龙器皿均需依次经沸腾王水与 Milli-Q 超纯水彻底清洗。所有浓度测量均采用单元素电感耦合等离子体质谱(ICP-MS)标准溶液 (Spex CertiPrep 公司, 质量浓度为 $1000 \pm 5 \mu\text{g/mL}$) (Tissot and Dauphas, 2015)。在铀同位素测试分析中, 离子交换树脂是实现样品前处理与纯化的关键材料, 其分离效果直接

决定最终同位素比值测量的精度与可靠性。该类树脂能从复杂基体中选择性吸附铀, 实现铀与干扰元素的分离及浓度富集, 从而为后续质谱分析提供高纯度铀溶液。该纯化过程可有效去除基体效应、多原子离子干扰及氧化物干扰等潜在影响因素, 降低同位素比值计算误差, 确保测定结果准确。目前广泛使用的离子交换树脂包括 TRU-Spec 树脂 (Luo

Xiaozhong et al., 1997; Stirling et al., 2007; Andersen et al., 2015) 和 U-TEVA 树脂 (Horwitz et al., 1992; Weyer et al., 2008; Tissot and Dauphas, 2015)。

2.2 分析测试与校正

$^{238}\text{U}/^{235}\text{U}$ 的初始比值 (138.9 ± 1.4) 最早由 Nier (1939) 在 20 世纪 30 年代通过热电离质谱仪 (TIMS) 分析一系列铀矿样品获得。此后, 铀同位素的测量精度逐步提高, 所需样品量也逐渐减少。20 世纪 70 年代, Cowan and Adler (1976) 采用气相色谱—质谱联用技术 (GC—MS) 并结合气态 UF_6 分析铀矿石样品, 将该比值的相对误差提高至 $\pm 0.2\%$ (Hamer and Robbins, 1960)。进入 80 年代, Chen Jinghua and Wasserburg (1980) 基于“Lunatic I”型 TIMS 对分析方法进行了重要改进: 通过引入 $^{238}\text{U}/^{235}\text{U}$ 双稀释剂校正仪器质量分馏, 不仅将相对误差提升至千分位 ($\%$) 水平, 还样品消耗量降至纳克级别。21 世纪以来, 随着 ^{236}U — ^{233}U 双稀释剂的广泛应用与质谱技术的持续进步, 多接收电感耦合等离子体质谱 (MC-ICPMS) 方法进一步将 $^{238}\text{U}/^{235}\text{U}$ 的测量精度提升至 $< \pm 0.1\%$, 样品用量亦降至 100 ng 以下 (Stirling et al., 2007; Weyer et al., 2008; Brennecka et al., 2010; Andersen et al., 2015; Tissot and Dauphas, 2015; Wang Xiangli et al., 2015)。此外, 在法拉第杯配置 $10^{10}\Omega$ 与 $10^{11}\Omega$ 的混合高阻阵列, 可显著增强 ^{235}U 的信号强度, 从而获得更优的信噪比, 使相对误差进一步提高至 $< \pm 0.03\%$ (Andersen et al., 2015)。

2.3 标准物质

铀同位素测试中使用的标准物质主要源自美国国家标准与技术研究院 (NIST) 及欧盟标准物质与测量研究所 (IRMM), 常见的有 CRM-112a、SRM-960、CRM-129a、CRM-145、SRM-950a、IRM-184 和 REIMP-18a 等 (Stirling et al., 2007; Weyer et al., 2008; Bopp et al., 2009; Condon et al., 2010; Richter et al., 2010; Brennecka et al., 2011a)。其中, CRM-112a 是目前应用最为广泛的标准物质, 而 CRM-145 是其溶解制成, 二者的同位素组成一致。在铀同位素测试中, $^{238}\text{U}/^{235}\text{U}$ 比值通常以相对于 CRM-112a (或 CRM-145) 标准物质的 δ 形式表示, 其计算公式如下:

$$\delta^{238}\text{U}_{\text{CRM-112a}} = \left\{ \frac{\left[\frac{n(^{238}\text{U})}{n(^{235}\text{U})} \right]_{\text{样品}}}{\left[\frac{n(^{238}\text{U})}{n(^{235}\text{U})} \right]_{\text{CRM-112a}}} - 1 \right\} \times 1000\%$$

$$\delta^{238}\text{U}_{\text{CRM-145}} = \left\{ \frac{\left[\frac{n(^{238}\text{U})}{n(^{235}\text{U})} \right]_{\text{样品}}}{\left[\frac{n(^{238}\text{U})}{n(^{235}\text{U})} \right]_{\text{CRM-145}}} - 1 \right\} \times 1000\%$$

在缺乏 CRM-112a (或 CRM-145) 标准物质的国内实验室, 可通过标样换算方法确保铀同位素数据的准确性和可比性。例如, 首先将所有样品先以实验室自主制备的纯铀溶液 USTC-U 为基准, 得到 $\delta^{238}\text{U}_{\text{样品-USTC-U}}$ 。然后将检测前预先测定的 USTC-U 与 CRM-145 固定同位素偏差 ($\delta^{238}\text{U}_{\text{USTC-U-CRM-145}}$) 代入公式 $\delta^{238}\text{U}_{\text{CRM-145}} = \delta^{238}\text{U}_{\text{USTC-U}} + \delta^{238}\text{U}_{\text{USTC-U-CRM-145}}$, 最终计算得到以 CRM-145 为标准物质的 $\delta^{238}\text{U}$ 值 (Sheng Jiaru et al., 2024)。

3 主要地质储库的铀同位素构成

厘定不同地质储库的铀同位素组成, 是利用铀同位素开展示踪研究的基本前提。随着相关分析数据的持续积累和公开发表, 构建全球尺度的铀同位素数据库已成为当前研究的迫切需求。Uranium Isotope Database (UID) 是最新构建的专业化铀同位素数据库, 系统整合了近 80 年来发表的铀同位素数据, 所有数据均以标准物质 CRM-145 为基准进行统一校准, 可为相关研究提供标准化的数据支持 (访问地址: <https://isotoparium.org/uid>)。铀在地球各储库之间持续迁移与循环, 其大致路径如图 (6) 所示。

3.1 大陆地壳

估算大陆地壳的铀同位素组成时, 主要以花岗岩等常见地壳岩石 (Weyer et al., 2008; Telus et al., 2012; Tissot and Dauphas, 2015; Noordmann et al., 2016) 及锆石、独居石、磷灰石等重要含铀副矿物为研究对象 (Hiess et al., 2012)。Weyer et al. (2008) 的研究显示, 花岗岩的 $\delta^{238}\text{U}$ 值范围为 $-0.20\% \sim -0.46\%$; Telus et al. (2012) 对 I 型、S 型、A 型花岗岩开展分析, 发现大部分样品 $\delta^{238}\text{U}$ 值集中于 $-0.23\% \sim -0.40\%$ 。整体而言, 不同类型岩石, 例如酸性岩 (花岗岩及流纹岩)、中性岩 (花岗闪长岩、闪长岩、英安岩、安山岩及英云闪长岩) 和碱性岩 (正长岩及粗面岩) 等的 $\delta^{238}\text{U}$ 值差异极小 (Tissot and Dauphas, 2015; Noordmann et al., 2016)。基于上述研究, Tissot and Dauphas (2015) 综合前人数据, 并结合大陆地壳不同类型岩石的分布占比及各自铀含量, 最终得出大陆上地壳的 $\delta^{238}\text{U}$ 推荐值为 -0.29% 。

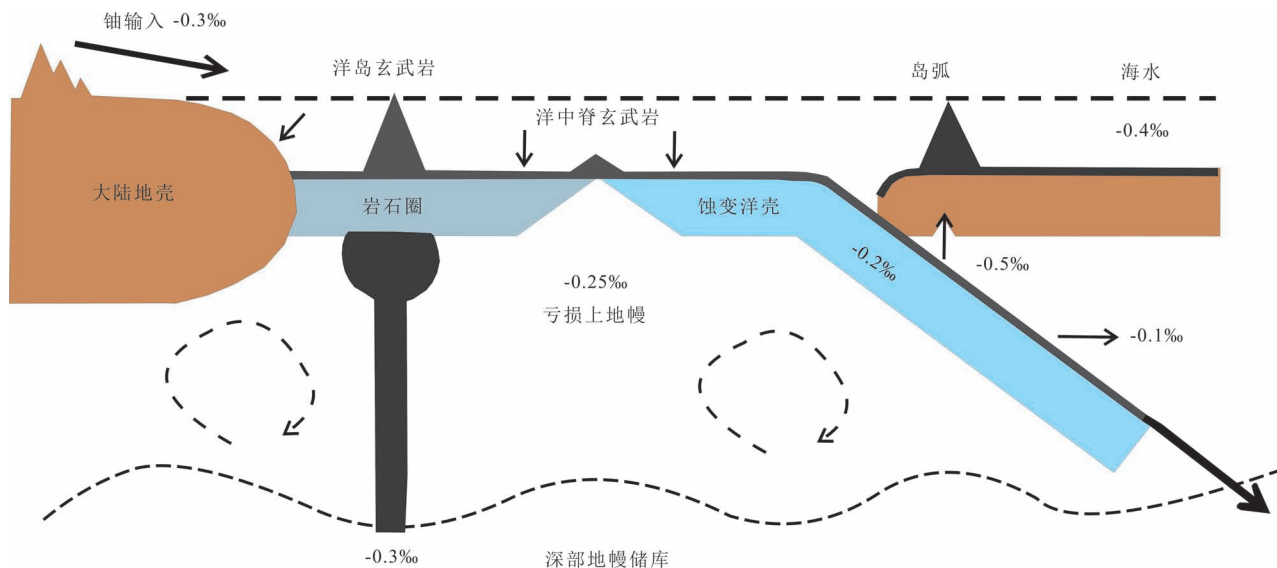


图 6 地球深部铀同位素 ($\delta^{238}\text{U}$) 现代循环示意图 (修改自 Andersen et al. , 2015)

Fig. 6 Modern cycle of uranium isotopes ($\delta^{238}\text{U}$) in the deep Earth (modified from Andersen et al. , 2015)

3.2 地幔

Weyer et al. (2008) 首次测得玄武岩样品的 $\delta^{238}\text{U}$ 值约为 -0.30‰ 。除单一玄武岩样品分析外, Andersen et al. (2015) 进一步针对洋岛玄武岩 (OIB)、大洋中脊玄武岩 (MORB) 及岛弧玄武岩 (IAB) 三类不同成因的玄武岩开展铀同位素系统研究, 进而提出上地幔铀同位素组成不均一的认识, 具体特征及成因解释如下: 在俯冲带中, 源自俯冲洋壳的脱水流体将同位素偏轻的铀 (富集 ^{235}U) 输送至岛弧, 导致岛弧玄武岩普遍具有较低的 $\delta^{238}\text{U}$ 值 (约 -0.38‰)。经流体提取后残留的俯冲物质, 其铀同位素组成则会偏重 (富集 ^{238}U)。这些重铀同位素随板片继续向深部迁移, 最终通过地幔对流等过程进入上地幔储库。当上地幔发生部分熔融形成洋中脊玄武岩时, 便混入了这类再循环的重铀组分, 致使洋中脊玄武岩整体表现出较高的 $\delta^{238}\text{U}$ 值 (约 -0.26‰)。相比之下, 洋岛玄武岩的源区来自更深部、受俯冲影响较小的地幔区域, 因此其 $\delta^{238}\text{U}$ 值更接近全硅酸盐地球的铀同位素组成 ($\delta^{238}\text{U} = -0.31\text{‰}$, Andersen et al. , 2017)。

3.3 海洋系统

海水中的 ^{238}U 相对于其输入通量而言表现为净亏损, 这种亏损可能主要由铀自海水的迁出过程所导致, 相关的汇包括: 还原性海洋 (如局限洋盆)、还原性沉积物、低温蚀变大洋洋壳、碳酸盐岩、铁锰结壳等 (图 7)。其中, 还原性海洋 (如局限洋盆)、还

原性沉积物、低温蚀变大洋洋壳、碳酸盐岩等相对富集 ^{238}U , 而金属沉积物 (如铁锰结核等) 则相对富集 ^{235}U , 造成了全球海水的铀同位素变化。

3.3.1 海水

铀在海洋中的滞留时间约为 0.40 Ma (Ku et al. , 1977), 远高于海水混合时间 (数百至数千年, Liu Camilla X et al. , 2024), 两者相差两个数量级以上, 因此海水铀同位素组成通常被视为高度均一。这一认识得到多项海水 $\delta^{238}\text{U}$ 研究的支持—除少数特殊环境外, 不同研究报道的海水 $\delta^{238}\text{U}$ 值在各自分析不确定度范围内基本一致 (Stirling et al. , 2007; Weyer et al. , 2008; Hiess et al. , 2012; Andersen et al. , 2014; Tissot and Dauphas, 2015)。例如, 夏威夷和百慕大海域海水的 $\delta^{238}\text{U}$ 值为 $-0.42\text{‰} \sim -0.38\text{‰}$ (平均 -0.41‰ , Weyer et al. , 2008), 而太平洋开放海域则为 $-0.40\text{‰} \sim -0.36\text{‰}$ (平均 -0.39‰ , Rolison et al. , 2017)。基于上述数据, Tissot and Dauphas (2015) 提出将 -0.39‰ 作为海水 $\delta^{238}\text{U}$ 的推荐平均值, 进一步确认了开放海域铀同位素的均一性。需要注意的是, 该结论主要适用于开放大洋环境。在黑海、波罗的海等部分缺氧海域的深层水体中 ($C(\text{O}_2) < 10^{-6} \text{ mol/L}$, Berner, 1981), 铀的还原过程与孔隙水扩散作用共同影响同位素组成, 导致 $\delta^{238}\text{U}$ 随水深增加而系统偏轻, 最低可达 -0.70‰ (Romaniello et al. , 2009; Noordmann et al. , 2015; Rolison et al. , 2017)。

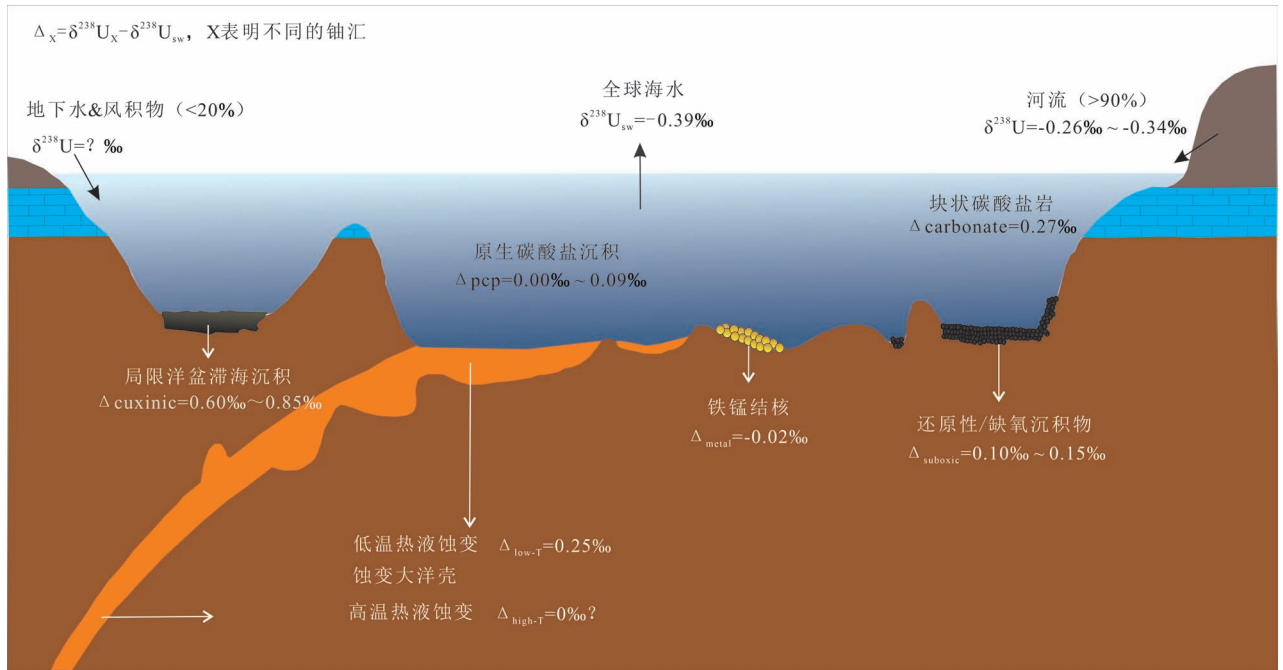


图7 海洋中铀同位素平衡模型(修改自罗劭侃等,2024)

Fig. 7 Equilibrium model of uranium isotopes in the ocean (modified after Luo Qukan et al., 2024)

海洋中主要的溶解铀来源于陆地河流,海洋铀汇包括还原性/缺氧沉积物、局限性滞海洋盆沉积、海相碳酸盐、铁锰结核及蚀变大洋壳
The main dissolved uranium in the ocean is derived from terrestrial rivers, and oceanic uranium is sequestered in reductive/anoxic sediments, restricted silled basin sediments, marine carbonates, ferromanganese nodules, and altered oceanic crust

3.3.2 还原性沉积物

海水中铀主要以 UO_2^{2+} 形式存在,并优先与碳酸根结合形成稳定络合物。受其高稳定性的影响,即便在缺氧条件下,水体中 U^{6+} 向 U^{4+} 的还原反应速率也较为缓慢(Anderson et al., 1989)。因此,铀的还原过程被认为主要发生在沉积物孔隙水或水—沉积物界面附近,且通常有微生物参与(Anderson et al., 1989; Klinkhammer and Palmer, 1991)。黑海、卡里亚科盆地等缺氧盆地的沉积物的 $\delta^{238}\text{U}$ 值介于 -0.2‰ 至 $+0.4\text{‰}$ 之间(Weyer et al., 2008; Montoya-Pino et al., 2010; Andersen et al., 2014; Noordmann et al., 2015; Hinojosa et al., 2016),显著高于海水和大陆地壳的平均 $\delta^{238}\text{U}$ 值。与之对应的是,这上覆深层水体的 $\delta^{238}\text{U}$ 值通常较低(Romaniello et al., 2009; Rolison et al., 2015),例如 Kyllaren Fjord 峡湾深部水体的 $\delta^{238}\text{U}$ 值可低至 -0.7‰ (Noordmann et al., 2015)。这种沉积物与水体之间的铀同位素分异,主要由两个关键过程共同驱动:一是在沉积物中铀发生部分还原并富集重同位素(如 ^{238}U),二是同位素较轻的铀同位素(如 ^{235}U) 向水体发生反向扩散(Nomura et al.,

1996; Fujii et al., 2006; Abe et al., 2008; Basu et al., 2014; Stirling et al., 2015; Stylo et al., 2015a, b; Wang Xiangli et al., 2015)。

3.3.3 海相碳酸盐

现有研究表明,原生碳酸盐的 $\delta^{238}\text{U}$ 值总体较为稳定,基本围绕海水 $\delta^{238}\text{U}$ 值小幅波动,平均值约为 $-0.40\text{‰} \pm 0.15\text{‰}$ (Stirling et al., 2007; Andersen et al., 2014, 2017)。这一特征说明,在碳酸钙从水体中沉淀的过程中,铀同位素产生的分馏有限(Chen Xinming et al., 2016)。然而,某些特定时期的碳酸盐显示出不同的铀同位素特征。例如,晚二叠世碳酸盐的 $\delta^{238}\text{U}$ 值显著偏轻,介于 -0.37‰ 至 -0.77‰ 之间,该异常可能与该时期的大洋缺氧事件有关(Brennecke et al., 2011a; Lau et al., 2016)。从垂向分布来看,随着埋藏深度增加,碳酸盐岩中铀的富集程度升高, $\delta^{238}\text{U}$ 值也随之增大(变化范围为 -0.24‰ 至 $+0.07\text{‰}$),且 $\delta^{238}\text{U}$ 值与铀含量大致呈正相关(Romaniello et al., 2013)。这一趋势可能与随深度加剧的缺氧环境有关—更强的还原条件促使沉积物与孔隙水之间发生铀同位素分馏,进而形成上述垂向分异模式(Andersen et al.,

2016)。此外,成岩作用也会显著影响碳酸盐的铀同位素组成。在白云石化过程中,碳酸盐岩的 $\delta^{238}\text{U}$ 值可能进一步偏轻,最低可达 -0.83‰ (Stirling et al., 2007)。

3.3.4 蚀变洋壳

大洋中脊玄武岩在蚀变过程中不仅会显著富集铀(Staudigel et al., 1996; Bach et al., 2003; Kelley et al., 2005),还会伴随显著的铀同位素分馏,其 $\delta^{238}\text{U}$ 值范围为 -0.46‰ 至 $+0.27\text{‰}$ (Andersen et al., 2015; Noordmann et al., 2016)。进一步研究表明,蚀变洋壳不同深度区段的 $\delta^{238}\text{U}$ 值存在系统性差异(Andersen et al., 2015):最上部岩层(0~110 m)样品的 $\delta^{238}\text{U}$ 值约为 -0.44‰ ,略低于海水;而110~420 m深度区间内的两个岩层样品则显示出明显偏高的 $\delta^{238}\text{U}$ 值,分别为 -0.14‰ 与 $+0.16\text{‰}$ 。这种差异可能与洋壳最上部未发生显著氧化还原反应、难以引发强烈铀同位素分馏有关。整体来看,蚀变洋壳的 $\delta^{238}\text{U}$ 值介于 -0.25‰ 至 -0.17‰ 之间,而对应热液流体的 $\delta^{238}\text{U}$ 值略低于海水。上述特征表明,海底低温蚀变作用($<100^\circ\text{C}$)倾向于优先从海水中移除重铀同位素(如 $\delta^{238}\text{U}$)(Andersen et al., 2015; Noordmann et al., 2016)。

3.3.5 铁锰氧化物

铁锰氧化物的 $\delta^{238}\text{U}$ 值分布范围较窄,介于 -0.71‰ 至 -0.52‰ 之间,平均值为 -0.62‰ (Stirling et al., 2007; Weyer et al., 2008; Goto et al., 2014; Wang Xiangli et al., 2016)。现有数据表明,铁锰氧化物的平均 $\delta^{238}\text{U}$ 值与其他含金属沉积物之间不存在系统性差异。这一特征说明海水与铁锰氧化物之间的铀同位素分馏较为稳定,其分馏幅度可表示为 $\Delta^{238}\text{U}_{(\text{海水}-\text{铁锰氧化物})} = 0.23\text{‰}$ 。此外,铀在铁锰氧化物表面的吸附过程也表现出类似的铀同位素分馏,对应的分馏系数为 $\Delta^{238}\text{U}_{(\text{海水}-\text{铁锰氧化物})} = 0.20\text{‰}$ (Brenneka et al., 2011b)。值得注意的是,多个铁锰结壳的深度剖面显示其 $\delta^{238}\text{U}$ 值在垂向基本保持不变,表明整个新生代期间海水的 $\delta^{238}\text{U}$ 组成可能相对稳定(Goto et al., 2014; Wang Xiangli et al., 2016)。

3.3.6 河流

受全球河流流域内地质单元组成差异的影响,河流铀同位素组成变化范围较大, $\delta^{238}\text{U}$ 值介于 -0.72‰ 至 $+0.06\text{‰}$ 之间(Andersen et al., 2014)。在流域尺度上,大型河流流域面积较广、覆盖多种地质单元,其铀同位素组成变化范围相对较窄, $\delta^{238}\text{U}$

值为 $-0.31\text{‰} \sim -0.13\text{‰}$,平均值为 -0.27‰ (Stirling et al., 2007; Noordmann et al., 2012, 2016; Andersen et al., 2014; Tissot and Dauphas, 2015)。相比之下,部分小型河流的铀同位素组成显著偏离河水平均值,可能与其流域面积小、受特定岩性(如黑色页岩)风化产物的强烈影响有关(Noordmann et al., 2012)。河水与大陆地壳的平均铀同位素差异较小,表明在地表氧化性风化过程中未发生显著的铀同位素分馏。Andersen et al. (2016)基于各河流的铀通量,计算出全球河流 $\delta^{238}\text{U}$ 的加权平均值为 -0.34‰ ;但该平均值受到长江极低 $\delta^{238}\text{U}$ 值(-0.70‰)的显著影响。若将长江从统计样本中剔除,全球河流 $\delta^{238}\text{U}$ 平均值将升至 -0.26‰ 。进一步来看,上地壳覆盖物的铀同位素组成存在显著差异:白云岩、蒸发岩和氧化物的 $\delta^{238}\text{U}$ 值通常极低($<-0.6\text{‰}$)(Stirling et al., 2007; Weyer et al., 2008; Romaniello et al., 2013; Goto et al., 2014; Tissot and Dauphas, 2015; Wang Xiangli et al., 2016),而黑色页岩与碳酸盐岩则可能呈现同位素偏重特征,其 $\delta^{238}\text{U}$ 值可达 $\geq 0.0\text{‰}$ (Weyer et al., 2008; Romaniello et al., 2013; Andersen et al., 2014)。这种差异有助于解释不同河流的同位素特征。例如,长江流域广泛分布同位素偏轻的蒸发岩和白云岩(Brenneka et al., 2011a),可能是其 $\delta^{238}\text{U}$ 值显著负值的原因;而印度河流域因富含黑色页岩,其 $\delta^{238}\text{U}$ 值相对较高,为 -0.18‰ (Noordmann et al., 2016)。

3.3.7 地下水

目前关于地下水 $\delta^{238}\text{U}$ 组成的研究相对有限。Wang Xiangli et al. (2015)认为,在风化过程中 U^{4+} 的部分氧化不会引起显著的铀同位素分馏;然而,Stirling et al. (2007)的淋滤实验则显示,风化作用仍可能对地下水的铀同位素组成产生影响。例如,由地下水析出碳酸盐所形成的洞穴沉积物的 $\delta^{238}\text{U}$ 值变化范围较大($-0.70\text{‰} \sim +0.44\text{‰}$),这可能源于渗流水在运移过程中优先淋滤出 ^{235}U 和 ^{234}U (Stirling et al., 2007)。Cheng Hai et al. (2013)在石笋中同样观测到偏轻的铀同位素特征, $\delta^{238}\text{U}$ 值为 $-0.60\text{‰} \sim -0.30\text{‰}$,进一步支持了风化作用对地下水及相关次生沉积物铀同位素组成具有影响的认识。

将不同类型的铀矿床、岩石、矿物的 $\delta^{238}\text{U}$ 值进行汇总(图8),为后续铀同位素在矿床中的应用提供参考。

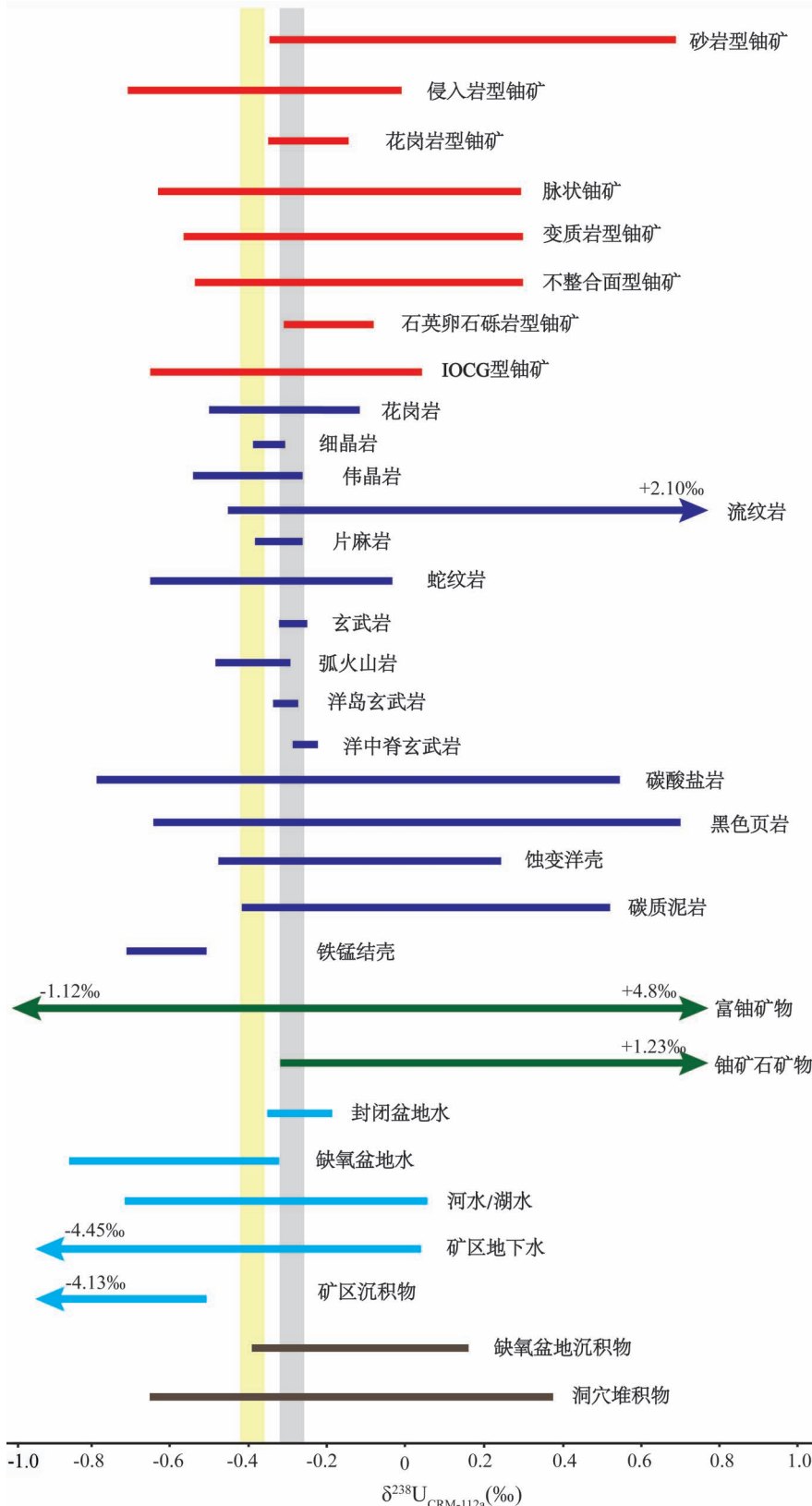


图 8 已发表文献中矿床、岩石、矿物、水和沉积物 $\delta^{238}\text{U}$ 值汇总
 Fig. 8 Summary of $\delta^{238}\text{U}$ values for geological reference materials of ore deposits, rocks, and minerals

红色、深蓝色、绿色、浅蓝色、褐色线条分别表示矿床、岩石、矿物、水和沉积物 $\delta^{238}\text{U}$ 值范围,黄色条带表示现代海水的铀同位素组成 ($\delta^{238}\text{U} = -0.39$),灰色条带表示大陆上地壳的铀同位素组成 ($\delta^{238}\text{U} = -0.29$)。数据来源 (Stirling et al., 2007; Weyer et al., 2008; Boppet et al., 2009; Montoya-Pino et al., 2010; Brennecka et al., 2010a,b, 2011a; Hiess et al., 2012; Telus et al., 2012; Asael et al., 2013; Kendall et al., 2015; Romaniello et al., 2013; Andersen et al., 2014, 2015, 2016; Dahl et al., 2014; Goto et al., 2014; Murphy et al., 2014; Uvarova et al., 2014; Goldmann et al., 2015; Brown et al., 2016; Chen Xinming et al., 2016, 2017, 2018; Kirchenbaur et al., 2016; Noordmann et al., 2016; Placzek et al., 2016; Wang Xiangli et al., 2016; Rolison et al., 2017; Spano et al., 2017; Tissot et al., 2017, 2019, 2021; Jemison et al., 2018; Livermore et al., 2018; Freymuth et al., 2019; Lewis et al., 2020; Keatley et al., 2021; Dang et al., 2022; Pavia et al., 2023; Voinot et al., 2024; Sheng Jiaru et al., 2025a, b)

Red, dark blue, green, light blue, and brown lines represent the $\delta^{238}\text{U}$ value ranges of ore deposits, rocks, minerals, water, and sediments, respectively. The yellow band indicates the uranium isotope composition of modern seawater ($\delta^{238}\text{U} = -0.39\text{‰}$), and the gray band indicates that of the upper continental crust ($\delta^{238}\text{U} = -0.29\text{‰}$). Data Sources (Stirling et al., 2007; Weyer et al., 2008; Boppet et al., 2009; Montoya-Pino et al., 2010; Brennecka et al., 2010a,b, 2011a; Hiess et al., 2012; Telus et al., 2012; Asael et al., 2013; Kendall et al., 2015; Romaniello et al., 2013; Andersen et al., 2014, 2015, 2016; Dahl et al., 2014; Goto et al., 2014; Murphy et al., 2014; Uvarova et al., 2014; Goldmann et al., 2015; Brown et al., 2016; Chen Xinming et al., 2016, 2017, 2018; Kirchenbaur et al., 2016; Noordmann et al., 2016; Placzek et al., 2016; Wang Xiangli et al., 2016; Rolison et al., 2017; Spano et al., 2017; Tissot et al., 2017, 2019, 2021; Jemison et al., 2018; Livermore et al., 2018; Freymuth et al., 2019; Lewis et al., 2020; Keatley et al., 2021; Dang et al., 2022; Pavia et al., 2023; Voinot et al., 2024; Sheng Jiaru et al., 2025a, b)

4 铀同位素在铀矿床研究中的应用

不同铀矿床类型表现出显著的 $\delta^{238}\text{U}$ 组成差异性。例如,高温氧化还原型、低温氧化还原型和非氧化还原型矿床之间均存在显著的铀同位素分异:砂岩型与岩浆热液型铀矿的 $\delta^{238}\text{U}$ 值差异可达约 1.0‰,而低温 (<200°C) 与高温 (>200°C) 铀矿之间也相差约 0.4‰ (Brennecka et al., 2010) (图 9)。这种差异可能与低温环境中 U^{6+} 还原为 U^{4+} 过程中发生的核体积效应有关 (Bopp et al., 2009; Lewis et al., 2020)。此外,低温矿床的 $^{238}\text{U}/^{235}\text{U}$ 值变化范围约为高温矿床的两倍,可能源于其局部环境的高变异性、更长的铀同位素分馏时间以及更低的形成温度 (Chernyshev et al., 2014)。因此,低温氧化还原过程是导致铀同位素值分异的主要原因。Uvarova et al. (2014) 对包括交代型、花岗岩型、钙结岩型、火山岩型、石英卵石砾岩型、砂岩型、不整合面型以及脉状铀矿在内的多种矿床进行了系统研究,发现其 $\delta^{238}\text{U}$ 值变化范围高达 1.8‰。不同类型矿

床铀矿物 $\delta^{238}\text{U}$ 值的差异主要受铀源同位素特征、 UO_2 体系中铀的还原效率以及铀从流体中迁出程度的影响;相比之下,成矿温度及后期蚀变作用的影响相对较小。这些特征表明,铀同位素在示踪自然体系氧化还原过程方面具有良好潜力。

除可用于区分矿床类型外,铀同位素在更小尺度也表现出显著变化。同一矿床中的不同脉体、同一脉体的不同位置,甚至单颗矿物内部均可观测到明显的 $\delta^{238}\text{U}$ 值波动 (Chernyshev et al., 2014; Keatley et al., 2021)。例如,同一矿脉或矿山采集的样品中, $\delta^{238}\text{U}$ 值范围可达 -0.16‰ ~ +0.03‰,这种差异可归因于氧化还原驱动的同位素分馏,以及局部淋滤与再沉淀过程中的铀再分配作用。研究还发现,在热液铀矿化过程中,晚期通过早期矿物相溶解—再沉淀形成的沥青铀矿,其 $\delta^{238}\text{U}$ 值通常比早期沥青铀矿轻约 0.46‰。铀在热液体系中通常以 U^{6+} 的形式迁移,在还原沉淀时, ^{238}U 倾向于进入早期形成的沥青铀矿,残余热液因此相对富集 ^{235}U 。随着成矿作用持续进行,后期沉淀的沥青铀矿便继

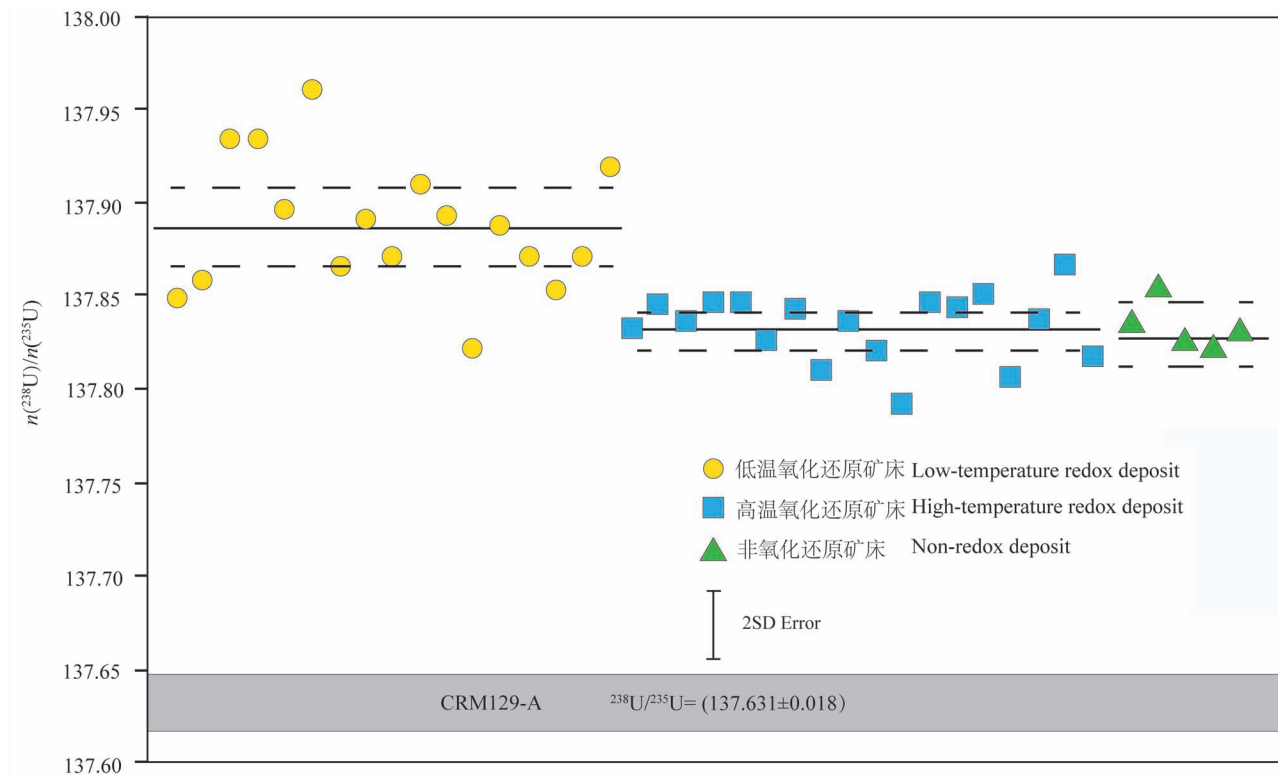


图 9 不同铀矿床类型及 $^{238}\text{U}/^{235}\text{U}$ 值 (据 Brennecka et al., 2010 修改)

Fig. 9 $^{238}\text{U}/^{235}\text{U}$ ratios of major uranium deposit types (modified from Brennecka et al., 2010)

实线代表分组平均值,虚线则表示每种铀矿类型的 2 倍标准偏差。CRM129-A 标准物质的 $^{238}\text{U}/^{235}\text{U}$ 值以灰色方框形式标注于图底部

The solid line represents the mean value for each uranium deposit type, while the dashed lines denote the ± 2 standard deviation (2σ).

The $^{238}\text{U}/^{235}\text{U}$ ratio of the CRM 129-A standard is shown as a grey box at the bottom of the figure

承了富集 ^{235}U 的特征,导致其 $\delta^{238}\text{U}$ 值降低。这一分馏趋势在多个矿床中得到印证,如俄罗斯 Krasnoyarsk Krai 地区的 Oktyabr' skii 矿床中,晚期沥青铀矿的 $^{238}\text{U}/^{235}\text{U}$ 值较早期降低 0.22‰ ~ 0.45‰;在加拿大 Saskatchewan 省的 Shea Creek 矿床中,该降低值可达约 0.46‰;而在澳大利亚 New South Wales 州的 Schlemma—Alberoda 矿床中,后期沉淀的铀硅石比早期沥青铀矿亦偏轻 0.31‰ (Chernyshev et al., 2014)。

4.1 砂岩型铀矿

砂岩型铀矿床形成于近地表常温环境,且赋存于渗透砂岩含水层的潜水面之下。砂岩型铀矿床成矿过程具鲜明的低温特征:源自地表的氧化性地下水渗入含水层后,携带着从上覆地层中淋滤出的水溶性铀酰向含水层系统更深处迁移;当这类氧化性地下水接触硫化物、有机质或碳氢化合物等还原剂时,溶解态 U^{6+} 会发生还原反应(过程可能由微生物介导),最终促使含 U^{4+} 的不溶性铀矿物沉淀,典型矿物包括沥青铀矿、铀石及其他以 U^{4+} 为主的单体铀矿物(Langmuir, 1978; Bargar et al., 2013)。因此,这些含 U^{4+} 的沉淀物会在氧化还原界面处富集,形成卷状砂岩型铀矿床(Kyser, 2014)。此类含 U^{4+} 的矿物可能发生后续再迁移。含水层中地下水的持续循环会导致铀矿物再溶解与再沉淀,进而推动氧化还原界面及矿化“卷状前缘”迁移(Hostetler and Garrels, 1962)。可见,在这种动态环境中,含 U^{6+} 和

含 U^{4+} 的矿物均可能发生化学沉淀。

在美国南德克萨斯州两处典型的“卷状铀矿床”中, $\delta^{238}\text{U}$ 值整体表现出从氧化带向还原带逐渐降低的趋势,这一分布特征可利用瑞利分馏模型解释—即铀矿物持续从已亏损 ^{238}U 的成矿流体中沉淀析出(Placzek et al., 2016)。在俄罗斯布里亚特共和国的 Dybryn 砂岩型铀矿床中, $^{238}\text{U}/^{235}\text{U}$ 比值与 $^{207}\text{Pb}/^{235}\text{U}$ 、 $^{206}\text{Pb}/^{238}\text{U}$ 测年结果呈显著正相关:成矿年龄偏老的样品,其 $^{238}\text{U}/^{235}\text{U}$ 比值相对较高。这一现象的成因,可能与成矿过程中 U^{6+} 还原为 U^{4+} 时的同位素分馏效应有关—此过程中 ^{238}U 更易在固相铀矿物中富集;而随成矿作用持续进行,晚期形成的铀矿物 ^{235}U 相对富集,导致其 $^{238}\text{U}/^{235}\text{U}$ 比值降低,对应较年轻的成矿年龄(Golubev et al., 2013)。Murphy et al. (2014)对高品位砂岩型铀矿中的沉积物及地下水进行了铀同位素分析,发现沉积物的 $\delta^{238}\text{U}$ 变化范围可达 5‰,而地下水的 $\delta^{238}\text{U}$ 变化范围约为 2‰。在 U^{6+} 还原为 U^{4+} 的过程中, ^{238}U 优先进入矿物晶格,造成地下水相对富集 ^{235}U ;随着铀不断从水体中迁出并沉淀,水相的 $^{238}\text{U}/^{235}\text{U}$ 比值逐渐向轻同位素方向偏移(图 10)。具体来说,砂岩型铀矿中的流体—矿物相互作用主要包括两类过程:一是铀矿物沉积之前,化学风化阶段从源岩中淋滤出铀;二是铀矿物沉淀之后经历热液蚀变。这两类过程均倾向于优先从矿物中迁出较轻的同位素 ^{235}U (Stirling et al., 2007; Hiess et al., 2012)。

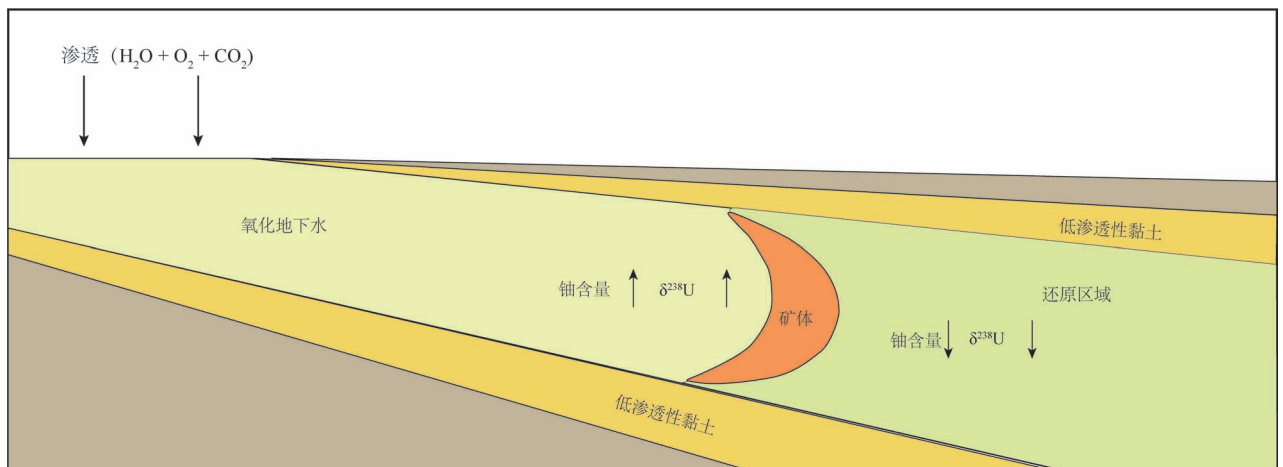


图 10 卷状铀矿床示意剖面图(修改自 Placzek et al., 2016)

Fig. 10 Schematic cross-section of roll front uranium deposits (modified from Placzek et al., 2016)

含有氧化剂的水体从矿物中析出铀元素,并将其携带至氧化还原界面。在该界面处,溶解态的铀发生沉淀,最终形成铀矿体,伴随铀品位和 $\delta^{238}\text{U}$ 值下降

Oxidant-bearing water leaches uranium from minerals and transports it to the redox interface. At this interface, dissolved uranium precipitates, eventually forming uranium orebodies, accompanied by decreases in uranium grade and $\delta^{238}\text{U}$ values

4.2 花岗岩型铀矿

花岗岩型铀矿的形成存在多种机制:既可通过结晶分异或部分熔融作用直接形成(Nash, 2009; Cuney, 2010, 2014),也可在岩浆岩侵位数百万年后,经由热液淋滤与活化铀形成后生矿床(Ruzicka, 1993; Hu et al., 2008; Cuney, 2009; Nash, 2010)。由于结晶分异过程对铀同位素分馏的影响较弱,所以热液作用被认为是控制铀同位素组成变化的关键因素(图 11)。在高温环境下,铀在流体与熔体之间的分配主要受非质量分馏(核体积效应)主导。具体表现为: ^{235}U 倾向于富集在含 U^{6+} 的矿物中,而 ^{238}U 则更易进入含 U^{4+} 矿物(Andersen et al., 2017; Tissot et al., 2019)。因此,岩浆热液因能有效溶解更多含 U^{6+} 的矿物而相对富集 ^{235}U (Chernyshev et al., 2014; Sheng et al., 2025a, b)。除价态外,铀的配体类型也会显著影响核体积效应所主导的同位素分馏(Abe et al., 2010)。在硅酸盐熔体中,铀主要以六价形式与氧结合(Farges et

al., 1992; Tissot et al., 2019);而在岩浆热液中,铀则倾向于与 F、Cl 等卤素形成络合物(Keppler and Wyllie, 1990; Peiffert et al., 1996)。值得注意的是,花岗岩型铀矿的成矿热液通常富 F 和 Cl (Ballouard et al., 2017; Zhang et al., 2022),这类组分可显著提升铀的迁移能力(Keppler and Wyllie, 1990; Peiffert et al., 1996)。

岩浆岩内部不同矿物之间可存在显著的铀同位素分馏。例如,源自同一母岩浆的榍石与锆石的 $\delta^{238}\text{U}$ 值差异可达 4.8‰;而不同产地、不同形成时代的岩浆锆石之间, $\delta^{238}\text{U}$ 值的变化范围亦可达 3.7‰(Tissot and Ibañez-Mejia, 2021)。在花岗岩系统中,共生的含 U^{4+} 矿物之间 $\delta^{238}\text{U}$ 值的变化范围可达 0.9‰。进一步观察表明,晚期沥青铀矿通常比早期阶段沥青铀矿具有更低的 $^{238}\text{U}/^{235}\text{U}$ 值,而晶质铀矿 $^{238}\text{U}/^{235}\text{U}$ 值的变化幅度则远小于沥青铀矿。这种铀同位素组成的差异性,很可能与矿床在演化过程中经历的多阶段成矿与再沉淀过程有关,而该过

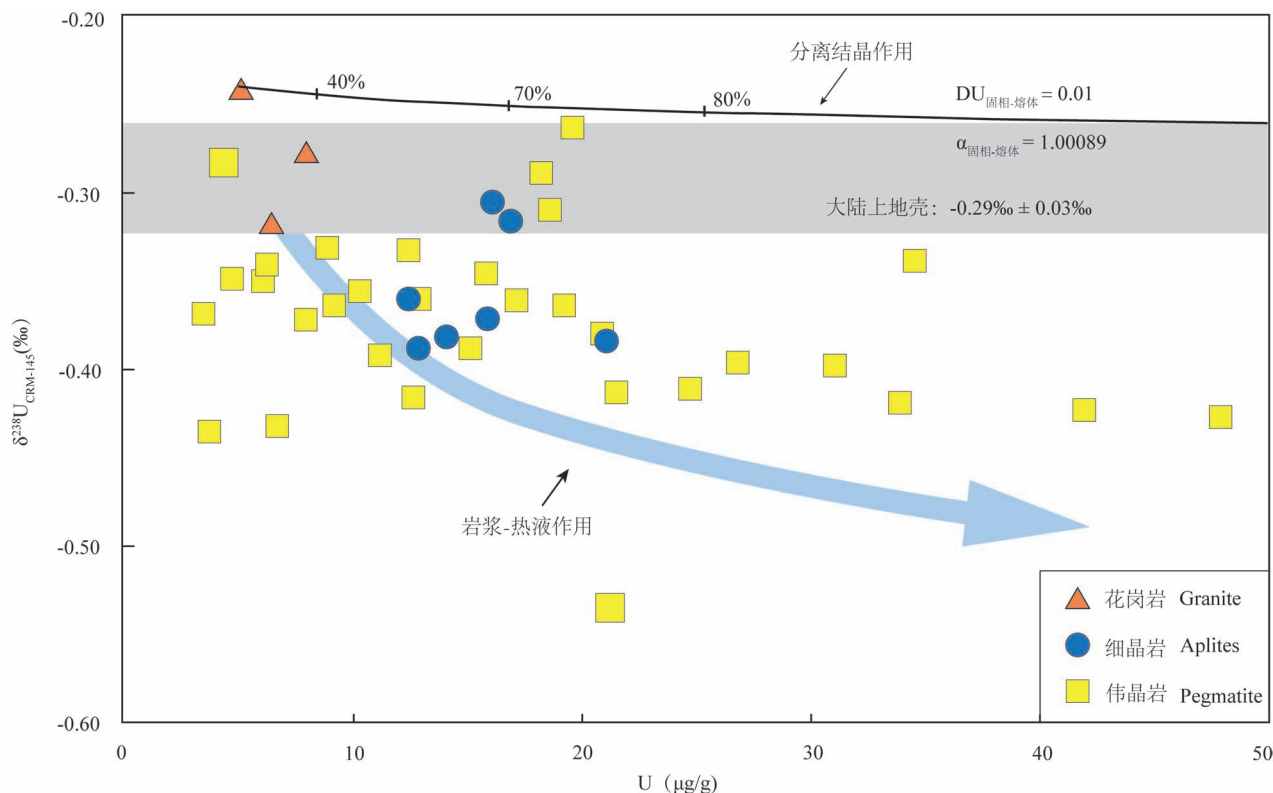


图 11 岩浆分离结晶过程和岩浆热液过程中 $\delta^{238}\text{U}$ 与铀含量关系图(修改自 Sheng et al., 2025b)

Fig. 11 Diagram of $\delta^{238}\text{U}$ vs. U content during magmatic fractional crystallization and magmatic—hydrothermal processes (modified after Sheng et al., 2025b)

曲线表示分步结晶过程中残余熔体内铀含量及铀同位素组成演化的模拟趋势,曲线标注数字指示结晶度

The curves represent the simulated evolution trends of U content and uranium isotopic composition in the residual melt during fractional crystallization, and the numbers marked on the curves indicate crystallinity

程伴随着温度、氧化还原条件等环境因素的改变 (Chernyshev et al., 2014)。

4.3 矿山修复

在铀矿山环境中,铀的释放主要来源于历史遗留矿山尾矿的自然溶出,以及原地浸出采矿技术等人为活动。当前已实施的修复策略的核心方法是在矿山地下水中直接注入改良试剂,促进高迁移性的 U^{6+} 还原为低迁移性的 U^{4+} 。生物修复是其中重要手段之一,其依赖于矿山系统中天然微生物群落介导 U^{4+} 的还原过程 (Anderson et al., 2003)。实验研究表明,在生物修复过程中,非晶质 U^{4+} 矿物种相较于晶质铀矿更易生成。然而,非晶质 U^{4+} 也更容易被氧化为 U^{6+} 并再次迁移,因此引发人们对铀污染场地修复效果长期稳定性的担忧。目前,这些修复策略的长期成效仍存在不确定性,需通过持续监测地下水水质来评估其实际成效。

在此背景下,铀同位素已展现出在铀矿山修复监测方面展现出巨大的潜力。 U^{6+} 向 U^{4+} 的还原过程

伴随显著的同位素分馏。例如,Basu et al. (2015) 和 Placzek et al. (2016) 在美国得克萨斯州南部的 Rosita 和 Kingsville Dome 原地浸出采区周边地下水中,观测到 $\delta^{238}U$ 变化范围超过 3‰; Brown et al. (2016) 在美国怀俄明州 Smith Ranch 采区也报道了类似规律。多数研究显示,沿地下水流方向,沉积物中 U^{6+} 浓度与 $\delta^{238}U$ 值均呈上升趋势,这可能反映了铀在流动时逐步还原并从水体中去除的过程 (Bopp et al., 2010; Murphy et al., 2014; Shiel et al., 2016) (图 12)。尽管不同研究中观测到的分馏因子存在差异,这可能与铀去除过程中的多种竞争机制有关,例如吸附与还原作用的相互竞争 (Brennecke et al., 2011b; Jemison et al., 2016, 2018; Roebbert et al., 2021),或生物与非生物还原过程途径共同作用的结果 (Dreissig et al., 2011; Wang Yuheng et al., 2013; Alessi et al., 2014)。上述研究均表明,铀同位素可作为识别矿山修复过程中铀还原区域的有效示踪工具,具备潜在的应用价值。

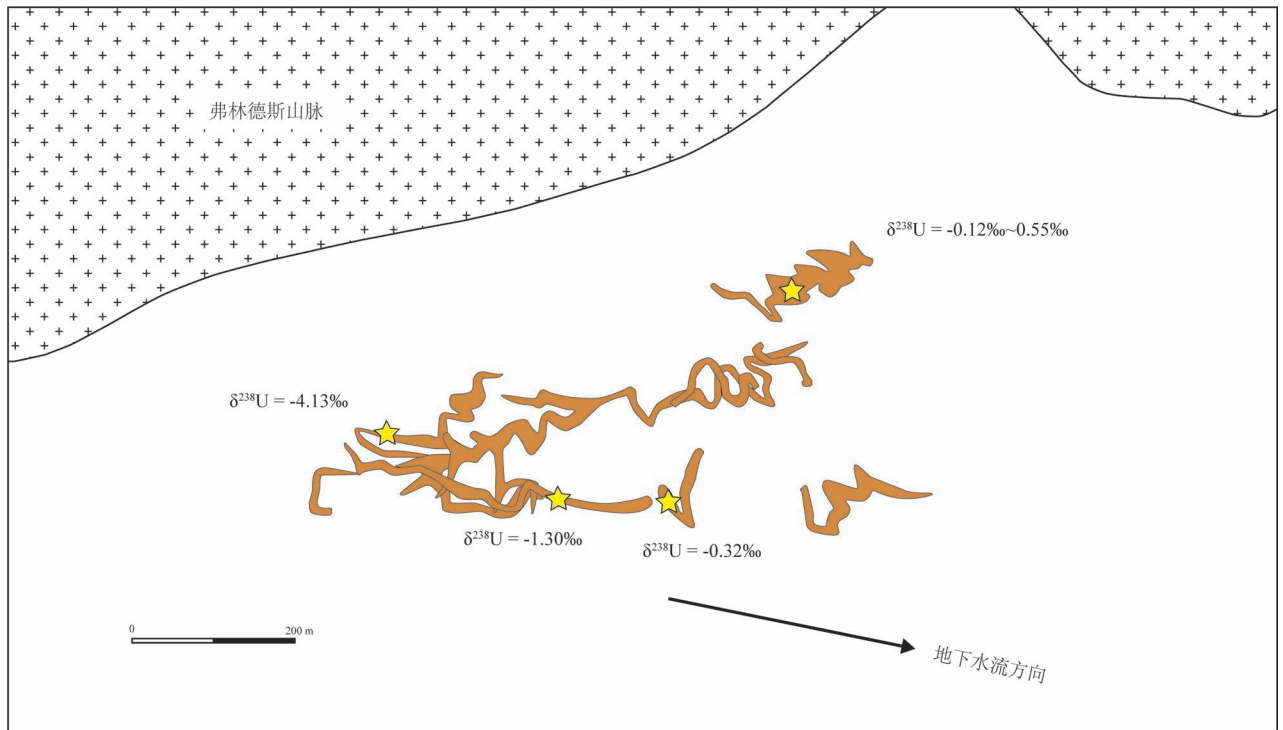


图 12 澳大利亚 Pepegooona 铀矿区沿地下水流方向上铀同位素富集变化特征 (修改自 Murphy et al., 2014)

Fig. 12 Characteristics of uranium isotope enrichment and variation along the groundwater flow path in Pepegooona uranium mining areas, Australia (modified after Murphy et al., 2014)

随着铀不断从水相迁出并沉淀至固相,矿化沉积物中重同位素的逐渐富集。这一现象证实地下水中 U^{6+} 去除过程中存在核体积效应与动力学瑞利分馏作用的共同影响

With uranium continuously migrating out of the aqueous phase and precipitating into the solid phase, the heavier isotopes in the mineralized sediments gradually become enriched. This phenomenon confirms the combined effects of the nuclear volume effect and kinetic Rayleigh fractionation during the removal of U^{6+} from groundwater

5 问题与展望

(1) 铀在氧化还原过程中的微观机制(如价电子转移路径与得失行为)如何影响其同位素分馏?核体积效应与质量依赖分馏在其中分别扮演何种角色?对铀同位素分馏机理的深入理解,是推动其在地球科学中应用的重要前提。

(2) 目前,铀同位素在示踪铀矿物质来源与成矿机制方面的研究仍较为缺乏。铀成矿过程常伴随显著的氧化还原反应,因此铀同位素在示踪成矿环境与过程方面具备天然优势。然而,现有研究多聚焦于分馏机制本身,针对矿床成因与成矿物质来源的同位素示踪研究仍然有限。铀同位素能否有效揭示成矿物质的来源及演化路径,目前尚不明确,亟需开展系统深入的工作。

(3) 铀同位素在高温地球化学过程中的应用尚处于起步阶段。与地表环境类似,地球深部过程(如地幔部分熔融、碳—硫循环和壳幔物质循环)同样涉及氧化还原反应,识别这些过程中的氧化还原变化对理解深部动力学机制至关重要。铀在高温条件下仍表现出以核体积效应为主导的显著同位素分馏,其质量相关分馏可忽略不计,这一特性明显不同于钼、铁等氧化还原敏感元素。因此,铀同位素有望为揭示地球深部过程提供新的视角与方法。

参 考 文 献 / References

(The literature whose publishing year followed by a “&” is in Chinese with English abstract; The literature whose publishing year followed by a “#” is in Chinese without English abstract)

陈振宇, 黄国龙, 朱捌, 陈郑辉, 黄凡, 赵正, 田泽瑾. 2014. 南岭地区花岗岩型铀矿的特征及其成矿专属性. *大地构造与成矿学*, 38(2): 264 ~ 275.

胡瑞忠, 骆金诚, 陈佑伟, 潘力川. 2019. 华南铀矿床研究若干进展. *岩石学报*, 35(9): 2625 ~ 2636.

李子颖, 秦明宽, 范洪海, 蔡煜琦, 程纪星, 郭冬发, 叶发旺, 范光, 刘晓阳. 2021. 我国铀矿地质科技近十年的主要进展. *矿物岩石地球化学通报*, 40(4): 845 ~ 857.

梁正伟, 田世洪. 2021. 铀“稳定”同位素分馏及其在地球科学中的应用. *地球科学*, 46(12): 4405 ~ 4426.

罗劭侃, 曹建华, 钟亮, 白冰, 王奇岗, 廖红为, 宗克清, 覃汉莲. 2024. 铀同位素反演古海洋环境的研究进展. *中国岩溶*, 43(4): 957 ~ 968.

骆金诚, 石少华, 陈佑伟, 田建吉. 2019. 铀矿床定年研究进展评述. *岩石学报*, 35(02): 589 ~ 605.

宋静, 谭凯旋, 刘振中, 李春光, 李咏梅, 翁宗翔. 2022. 自然界铀同位素分馏研究进展及展望. *核化学与放射化学*, 44(6): 565 ~ 574.

王大钊, 冷成彪, 秦朝建, 段丰浩, 周万蓬, 许德如. 2022. 铀的地球化学性质与成矿作用. *大地构造与成矿学*, 46(2): 282 ~

302.

杨莎, 刘耘. 2015. 铀稳定同位素核体积效应的理论研究. *矿物学报*, 35(S1): 1133.

张龙, 陈振宇, 汪方跃. 2021. 华南花岗岩型铀矿床主要特征与成矿作用研究进展. *岩石学报*, 37(9): 2657 ~ 2676.

张明林, 李胜祥, 刘悦, 郭庆银, 秦明宽, 车永飞. 2025. 全球铀矿勘查进展与展望. *地质论评*, 71(3): 1020 ~ 1028.

Abe M, Suzuki T, Fujii Y, Hada M, Hirao K. 2008. An ab initio molecular orbital study of the nuclear volume effects in uranium isotope fractionations. *The Journal of Chemical Physics*, 129(16): 1 ~ 7.

Acharya C and Apte S K. 2013. Novel surface associated polyphosphate bodies sequester uranium in the filamentous, marine cyanobacterium, *Anabaena torulosa*. *Metallomics*, 5(12): 1595 ~ 1598.

Acharya C, Chandwadkar P, Nayak C. 2017. Unusual versatility of the filamentous, diazotrophic cyanobacterium *Anabaena torulosa* revealed for its survival during prolonged uranium exposure. *Applied and Environmental Microbiology*, 83(9): e03356 ~ 03316.

Alessi D S, Lezama ~ Pacheco J S, Stubbs J E, Janousch M, Bargar J R, Persson P, Bernier-Latmani R. 2014. The product of microbial uranium reduction includes multiple species with U(IV) - phosphate coordination. *Geochimica et Cosmochimica Acta*, 131: 115 ~ 127.

Andersen M B, Elliott T, Freymuth H, Sims K W W, Niu Y, Kelley K A. 2015. The terrestrial uranium isotope cycle. *Nature*, 517(7534): 356 ~ 359.

Andersen M B, Romaniello S, Vance D, Little S H, Herdman R, Lyons T W. 2014. A modern framework for the interpretation of $^{238}\text{U}/^{235}\text{U}$ in studies of ancient ocean redox. *Earth and Planetary Science Letters*, 400: 184 ~ 194.

Andersen M B, Stirling C H, Weyer S. 2017. Uranium isotope fractionation. *Reviews in Mineralogy and Geochemistry*, 82(1): 799 ~ 850.

Andersen M B, Vance D, Morford J L, Bura-Naki E, Breitenbach S F M, Och L. 2016. Closing in on the marine $^{238}\text{U}/^{235}\text{U}$ budget. *Chemical Geology*, 420: 11 ~ 22.

Anderson R F, Fleisher M Q, LeHuray A P. 1989. Concentration, oxidation state, and particulate flux of uranium in the Black Sea. *Geochimica et Cosmochimica Acta*, 53(9): 2215 ~ 2224.

Anderson R T, Vronis H A, Ortiz-Bernad I, Resch C T, Long P E, Dayvault R, Karp K, Marutzky S, Metzler D R, Peacock A, White D C, Lowe M, Lovley D R. 2003. Stimulating the in situ activity of *Geobacter* species to remove uranium from the groundwater of a uranium ~ contaminated aquifer. *Applied Environmental Microbiology*, 69(10): 5884 ~ 5891.

Asael D, Tissot F L H, Reinhard C T, Rouxel O, Dauphas N, Lyons T W, Ponzevera E, Liorzou C, Chéron S. 2013. Coupled molybdenum, iron and uranium stable isotopes as oceanic paleoredox proxies during the Paleoproterozoic Shunga Event. *Chemical Geology*, 362: 193 ~ 210.

Bach W, Peucker-Ehrenbrink B, Hart S R, Blusztajn J S. 2003. Geochemistry of hydrothermally altered oceanic crust: DSDP/ODP Hole 504B - Implications for seawater-crust exchange budgets and Sr- and Pb- isotopic evolution of the mantle. *Geochemistry, Geophysics, Geosystems*, 4(3): 1 ~ 29.

Ballouard C, Poujol M, Boulvais P, Mercadier J, Tartèse R, Venneman T, Delouie E, Jolivet M, Kéré I, Cathelineau M, Cuney M. 2017.

- Magmatic and hydrothermal behavior of uranium in syntectonic leucogranites: The uranium mineralization associated with the Hercynian Guérande granite (Armorican Massif, France). *Ore Geology Reviews*, 80: 309 ~ 331.
- Bargar J R, Williams K H, Campbell K M, Long P E, Stubbs J E, Suvorova E I, Lezama-Pacheco J S, Alessi D S, Stylo M, Webb S M, Davis J A, Giammar DE, Blue LY, Bernier-Latmani R. 2013. Uranium redox transition pathways in acetate-amended sediments. *Proceedings of the National Academy of Sciences*, 110(12): 4506 ~ 4511.
- Basu A, Brown S T, Christensen J N, DePaolo D J, Reimus P W, Heikoop J M, Woldegabriel G, Simmons A M, House B M, Hartmann M, Maher K. 2015. Isotopic and geochemical tracers for U(VI) reduction and U mobility at an in situ recovery U mine. *Environmental Science & Technology*, 49(10): 5939 ~ 5947.
- Basu A, Sanford R A, Johnson T M, Lundstrom C C, Löffler F E. 2014. Uranium isotopic fractionation factors during U(VI) reduction by bacterial isolates. *Geochimica et Cosmochimica Acta*, 136: 100 ~ 113.
- Basu A, Wanner C, Johnson T M, Lundstrom C C, Sanford R A, Sonnenthal E L, Boyanov M I, Kemner K M. 2020. Microbial U isotope fractionation depends on the U(VI) reduction rate. *Environmental Science & Technology*, 54(4): 2295 ~ 2303.
- Berner RA. 1981. A new geochemical classification of sedimentary environments. *Journal of Sedimentary Research*, 51(2): 359 ~ 365.
- Bigeleisen J. 1996. Nucleus size and shape effects in chemical reactions. *Isotope Chemistry of the Heavy Elements*. *Journal of the American Chemical Society*, 118(15): 3676 ~ 3680.
- Bigeleisen J. 1998. Second-order correction to the Bigeleisen - Mayer equation due to the nuclear field shift. *Proceedings of the National Academy of Sciences*, 95(9): 4808 ~ 4809.
- Bopp C J, I V, Lundstrom C C, Johnson T M, Glessner J J G. 2009. Variations in $^{238}\text{U}/^{235}\text{U}$ in uranium ore deposits: Isotopic signatures of the U reduction process? *Geology*, 37(7): 611 ~ 614.
- Bopp C J, Lundstrom C C, Johnson T M, Sanford R A, Long P E, Williams K H. 2010. Uranium $^{238}\text{U}/^{235}\text{U}$ isotope ratios as indicators of reduction; results from an in situ biostimulation experiment at Rifle, Colorado, U. S. A. *Environmental Science & Technology*, 44(15): 5927 ~ 5933.
- Brennecka G A, Borg L E, Hutcheon I D, Sharp M A, Anbar A D. 2010. Natural variations in uranium isotope ratios of uranium ore concentrates: Understanding the $^{238}\text{U}/^{235}\text{U}$ fractionation mechanism. *Earth and Planetary Science Letters*, 291(1): 228 ~ 233.
- Brennecka G A, Herrmann A D, Algeo T J, Anbar A D. 2011a. Rapid expansion of oceanic anoxia immediately before the end ~ Permian mass extinction. *Proceedings of the National Academy of Sciences*, 108(43): 17631 ~ 17634.
- Brennecka G A, Wasylenki L E, Bargar J R, Weyer S, Anbar A D. 2011b. Uranium isotope fractionation during adsorption to Mn-oxhydroxides. *Environmental Science & Technology*, 45(4): 1370 ~ 1375.
- Brown S T, Basu A, Christensen J N, Reimus P, Heikoop J, Simmons A, Woldegabriel G, Maher K, Weaver K, Clay J, DePaolo D J. 2016. Isotopic Evidence for Reductive Immobilization of Uranium Across a Roll-Front Mineral Deposit. *Environmental Science & Technology*, 50(12): 6189 ~ 6198.
- Brown S T, Basu A, Ding Xin, Christensen J N, DePaolo D J. 2018. Uranium isotope fractionation by abiotic reductive precipitation. *Proceedings of the National Academy of Sciences*, 115(35): 8688 ~ 8693.
- Catalano J G and Brown G E. 2005. Uranyl adsorption onto montmorillonite: Evaluation of binding sites and carbonate complexation. *Geochimica et Cosmochimica Acta*, 69(12): 2995 ~ 3005.
- Chen Junhui and Wasserburg G J. 1980. A search for isotopic anomalies in uranium. *Geophysical Research Letters*, 7(4): 275 ~ 278.
- Chen Xinming, Romaniello S J, Anbar A D. 2017. Uranium isotope fractionation induced by aqueous speciation: Implications for U isotopes in marine CaCO_3 as a paleoredox proxy. *Geochimica et Cosmochimica Acta*, 215: 162 ~ 172.
- Chen Xinming, Romaniello S J, Herrmann A D, Samankassou E, Anbar A D. 2018. Biological effects on uranium isotope fractionation ($^{238}\text{U}/^{235}\text{U}$) in primary biogenic carbonates. *Geochimica et Cosmochimica Acta*, 240: 1 ~ 10.
- Chen Xinming, Romaniello S J, Herrmann A D, Wasylenki L E, Anbar A D. 2016. Uranium isotope fractionation during coprecipitation with aragonite and calcite. *Geochimica et Cosmochimica Acta*, 188: 189 ~ 207.
- Chen Xinming, Zheng W, Anbar A D. 2020. Uranium Isotope Fractionation ($^{238}\text{U}/^{235}\text{U}$) during U(VI) Uptake by Freshwater Plankton. *Environmental Science & Technology*, 54(5): 2744 ~ 2752.
- Chen Zhenyu, Huang Guolong, Zhu Ba, Chen Zhenghui, Huang Fan, Zhao Zheng, Tian Zejin. 2014. The characteristics and metallogenic specialization of granite-hosted uranium deposits in the Nanling region. *Geotectonica et Metallogenia*, 38(2): 264 ~ 275.
- Cheng Hai, Edwards R L, Shen C C, Polyak V J, Asmerom Y, Woodhead J, Hellstrom J, Wang Yongjin, Kong Xinggong, Spittl C, Wang X, Calvin A E. 2013. Improvements in ^{230}Th dating, ^{230}Th and ^{234}U half-life values, and U-Th isotopic measurements by multi-collector inductively coupled plasma mass spectrometry. *Earth and Planetary Science Letters*, 371~372: 82 ~ 91.
- Chernyshev I V, Golubev V N, Chugaev A V, Baranova A N. 2014. $^{238}\text{U}/^{235}\text{U}$ isotope ratio variations in minerals from hydrothermal uranium deposits. *Geochemistry International*, 52(12): 1013 ~ 1029.
- Condon D J, McLean N, Noble S R, Bowring S A. 2010. Isotopic composition ($^{238}\text{U}/^{235}\text{U}$) of some commonly used uranium reference materials. *Geochimica et Cosmochimica Acta*, 74(24): 7127 ~ 7143.
- Cowan G A and Adler H H. 1976. The variability of the natural abundance of ^{235}U . *Geochimica et Cosmochimica Acta*, 40(12): 1487 ~ 1490.
- Cuney M. 2009. The extreme diversity of uranium deposits. *Mineralium Deposita*, 44(1): 3 ~ 9.
- Cuney M. 2010. Evolution of Uranium Fractionation Processes through Time: Driving the Secular Variation of Uranium Deposit Types. *Economic Geology*, 105(3): 553 ~ 569.
- Cuney M. 2014. Felsic magmatism and uranium deposits. *Bulletin de la Société Géologique de France*, 185(2): 75 ~ 92.
- Dahl T W, Boyle R A, Canfield D E, Connelly J N, Gill B C, Lenton T M, Bizzarro M. 2014. Uranium isotopes distinguish two geochemically distinct stages during the later Cambrian SPICE event. *Earth and Planetary Science Letters*, 401: 313 ~ 326.

- Dang D H, Novotnik B, Wang Wei, Georg R B, Evans R D. 2016. Uranium isotope fractionation during adsorption, (Co)precipitation, and biotic reduction. *Environmental Science & Technology*, 50(23): 12695 ~ 12704.
- Dang D H, Wang Wei, Gibson T M, Kunzmann M, Andersen M B, Halverson G P, Evans RD. 2022. Authigenic uranium isotopes of late Proterozoic black shale. *Chemical Geology*, 588: 1 ~ 11.
- Dieng S, Kyser K, Godin L. 2013. Tectonic history of the North American shield recorded in uranium deposits in the Beaverlodge area, northern Saskatchewan, Canada. *Precambrian Research*, 224: 316 ~ 340.
- Dieng S, Kyser K, Godin L. 2015. Genesis of multifarious uranium mineralization in the Beaverlodge Area, Northern Saskatchewan, Canada. *Economic Geology*, 110(1): 209 ~ 240.
- Dreissig I, Weiss S, Hennig C, Bernhard G, Zänker H. 2011. Formation of uranium (IV)—silica colloids at near-neutral pH. *Geochimica et Cosmochimica Acta*, 75(2): 352 ~ 367.
- Fang Tong and Liu Yun. 2019. Equilibrium thallium isotope fractionation and its constraint on Earth's late veneer. *Acta Geochimica*, 38(4): 459 ~ 471.
- Farges F, Ponader C W, Calas G, Brown G E. 1992. Structural environments of incompatible elements in silicate glass/melt systems; II. UIV, UV, and UVI. *Geochimica et Cosmochimica Acta*, 56(12): 4205 ~ 4220.
- Florence T M, Batley G E, Ekstrom A, Fardy J J, Farrar Y J. 1975. Separation of uranium isotopes by uranium (IV) — uranium (VI) chemical exchange. *Journal of Inorganic and Nuclear Chemistry* 37(9): 1961 ~ 1966.
- Freythuth H, Andersen MB, Elliott T. 2019. Uranium isotope fractionation during slab dehydration beneath the Izu arc. *Earth and Planetary Science Letters*, 522: 244 ~ 254.
- Fujii Y, Higuchi N, Haruno Y, Nomura M, Suzuki T. 2006. Temperature dependence of isotope effects in uranium chemical exchange reactions. *Journal of Nuclear Science and Technology*, 43: 400 ~ 406.
- Fujii Y, Nomura M, Okamoto M, Onitsuka H, Kawakami F, Takeda K. 1989a. Anomalous isotope effect of ^{235}U in U(IV)—U(VI) chemical exchange. *Zeitschrift für Naturforschung A*, 44: 395 ~ 398.
- Fujii Y, Nomura M, Onitsuka H, Takeda K. 1989b. Anomalous isotope fractionation in uranium enrichment process. *Journal of Nuclear Science and Technology*, 26: 1061 ~ 1064.
- Gagné J M, Saint-Dizier J P, Pianarosa P. 1977. Odd-even staggering of ^{235}U from the 5027 Å line in U I. *Optics Communications*, 20(2): 269 ~ 270.
- Gagné J M, Saint-Dizier J P, Pianarosa P. 1978. Isotope shift ^{238}U — ^{233}U from some lines in the UI spectrum. *Optics Communications*, 26(3): 348 ~ 350.
- Gagné J M, Van S N, Saint-Dizier J P, Pianarosa P. 1976. Isotope shift of ^{234}U , ^{236}U , ^{238}U in U. *Journal of the Optical Society of America*, 66(12): 1415 ~ 1416.
- Goldmann A, Brennecke G, Noordmann J, Weyer S, Wadhwa M. 2015. The uranium isotopic composition of the Earth and the Solar System. *Geochimica et Cosmochimica Acta*, 148: 145 ~ 158.
- Golubev V N, Chernyshev I V, Chugaev A V, Eremina A V, Baranova A N, Krupskaya V V. 2013. U ~ Pb systems and U isotopic composition of the sandstone-hosted paleovalley Dybryn uranium deposit, Vitim uranium district, Russia. *Geology of Ore Deposits*, 55(6): 399 ~ 410.
- Goto K T, Anbar A D, Gordon G W, Romaniello S J, Shimoda G, Takaya Y, Tokumaru A, Nozaki T, Suzuki K, Machida S, Hanyu T, Usui A. 2014. Uranium isotope systematics of ferromanganese crusts in the Pacific Ocean: Implications for the marine $^{238}\text{U}/^{235}\text{U}$ isotope system. *Geochimica et Cosmochimica Acta*, 146: 43 ~ 58.
- Greathouse J A, O'Brien R J, Bemis G, Pabalan R T. 2002. Molecular Dynamics Study of Aqueous Uranyl Interactions with Quartz (010). *The Journal of Physical Chemistry B*, 106(7): 1646 ~ 1655.
- Hamer A N and Robbins E J. 1960. A search for variations in the natural abundance of uranium-235. *Geochimica et Cosmochimica Acta*, 19(2): 143 ~ 145.
- Hiess J, Condon D J, McLean N, Noble S R. 2012. $^{238}\text{U}/^{235}\text{U}$ systematics in terrestrial uranium-bearing minerals. *Science*, 335(6076): 1610 ~ 1614.
- Hinojosa J L, Stirling C H, Reid M R, Moy C M, Wilson G S. 2016. Trace metal cycling and $^{238}\text{U}/^{235}\text{U}$ in New Zealand's fjords: Implications for reconstructing global paleoredox conditions in organic-rich sediments. *Geochimica et Cosmochimica Acta*, 179: 89 ~ 109.
- Horwitz E P, Dietz M L, Chiarizia R, Diamond H, Essling A M, Graczyk D. 1992. Separation and preconcentration of uranium from acidic media by extraction chromatography. *Analytica Chimica Acta*, 266(1): 25 ~ 37.
- Hostetler P B, Garrels R M. 1962. Transportation and precipitation of uranium and vanadium at low temperatures, with special reference to sandstone-type uranium deposits. *Economic Geology*, 57(2): 137 ~ 167.
- Hu Ruizhong, Bi Xianwu, Zhou Meifu, Peng Jiantang, Su Wenchao, Liu Shen, Qi Hhuawen. 2008. Uranium metallogenesis in south China and its relationship to crustal extension during the Cretaceous to Tertiary. *Economic Geology*, 103(3): 583 ~ 598.
- Hu Ruizhong, Luo Jincheng, Chen Youwei, Pan Lichuan. 2019. Several progresses in the study of uranium deposits in South China. *Acta Petrologica Sinica*, 35(9): 2625 ~ 2636.
- Jaffey A H, Flynn K F, Glendenin L E, Bentley W C, Essling A M. 1971. Precision Measurement of Half-Lives and Specific Activities of ^{235}U and ^{238}U . *Physical Review C*, 4(5): 1889 ~ 1906.
- Jemison N E, Johnson T M, Shiel A E, Lundstrom C C. 2016. Uranium isotopic fractionation induced by U(VI) adsorption onto common aquifer minerals. *Environmental Science & Technology*, 50(22): 12232 ~ 12240.
- Jemison N E, Shiel A E, Johnson T M, Lundstrom C C, Long P E, Williams K H. 2018. Field application of $^{238}\text{U}/^{235}\text{U}$ measurements to detect reoxidation and mobilization of U(IV). *Environmental Science & Technology*, 52(6): 3422 ~ 3430.
- Keatley A C, Dunne J A, Martin T L, Nita D C, Andersen M B, Scott T B, Richards D A, Awbery R P. 2021. Uranium isotope variation within vein-type uranium ore deposits. *Applied Geochemistry*, 131: 104977.
- Kelley K A, Plank T, Farr L, Ludden J, Staudigel H. 2005. Subduction cycling of U, Th, and Pb. *Earth and Planetary Science Letters*, 234(3): 369 ~ 383.
- Kendall B, Komiya T, Lyons T W, Bates S M, Gordon G W, Romaniello S J, Jiang G, Creaser R A, Xiao Shuhai, McFadden K, Sawaki Y, Tahata M, Shu Degan, Han Jian, Li Yong, Chu Xuelei, Anbar AD. 2015. Uranium and molybdenum isotope evidence for an episode of widespread ocean oxygenation during the late Ediacaran

- Period. *Geochimica et Cosmochimica Acta*, 156: 173 ~ 193.
- Keppeler H and Wyllie P J. 1990. Role of fluids in transport and fractionation of uranium and thorium in magmatic processes. *Nature*, 348(6301): 531 ~ 533.
- Kirchenbaur M, Maas R, Ehrig K, Kamenetsky V S, Strub E, Ballhaus C, Münker C. 2016. Uranium and Sm isotope studies of the supergiant Olympic Dam Cu - Au - U - Ag deposit, South Australia. *Geochimica et Cosmochimica Acta*, 180: 15 ~ 32.
- Klinkhammer G P and Palmer M R. 1991. Uranium in the oceans: Where it goes and why. *Geochimica et Cosmochimica Acta*, 55(7): 1799 ~ 1806.
- Knyazev D A, Myasoedov N F. 2001. Specific effects of heavy nuclei in chemical equilibrium. *Separation Science and Technology*, 36(8~9): 1677 ~ 1696.
- Ku T L, Mathieu G G, Knauss K G. 1977. Uranium in open ocean: concentration and isotopic composition. *Deep Sea Research*, 24(11): 1005 ~ 1017.
- Kyser K. 2014. Uranium ore deposits. *Treatise on Geochemistry* (Second Edition), 13(10): 489 ~ 513.
- Langmuir D. 1978. Uranium solution—mineral equilibria at low temperatures with applications to sedimentary ore deposits. *Geochimica et Cosmochimica Acta*, 42(6, Part A): 547 ~ 569.
- Lau K V, Maher K, Altiner D, Kelley B M, Kump L R, Lehrmann D J, Silva-Tamayo J C, Weaver K L, Yu M, Payne J L. 2016. Marine anoxia and delayed Earth system recovery after the end ~ Permian extinction. *Proceedings of the National Academy of Sciences*, 113(9): 2360 ~ 2365.
- Lewis S R, Simonetti A, Corcoran L, Simonetti S S, Dorais C, Burns P C. 2020. The role of continental crust in the formation of uraninite-based ore deposits. *Minerals*, 10(2): 1 ~ 27.
- Li Haoyu and Tissot F L H. 2023. UID: The uranium isotope database. *Chemical Geology*, 618: 121221.
- Li Ziyang, Qin Mingkuan, Fan Honghai, Cai Yuqi, Cheng Jixing, Guo Dongfa, Ye Fawang, Fan Guang, Liu Xiaoyang. 2021. Main progresses of uranium geology and exploration techniques for the past decade in China. *Bulletin of Mineralogy, Petrology and Geochemistry*, 40(4): 845 ~ 857.
- Liang Zhengwei and Tian Shihong. 2021. Uranium “Stable” isotope fractionation and its applications in Earth science. *Earth Science*, 46(12): 4405 ~ 4426.
- Liu Camillar X, Capirala A, Olson S L, Jansen M F, Dauphas N. 2024. Ocean mixing timescale through time and implications for the origin of iron formations. *Geochemical Perspectives Letters*, 31: 54 ~ 59.
- Livermore B D, Connelly J N, Moynier F, Bizzarro M. 2018. Evaluating the robustness of a consensus $^{238}\text{U}/^{235}\text{U}$ value for U—Pb geochronology. *Geochimica et Cosmochimica Acta* 237: 171 ~ 183.
- Luo Suisui and Gu Baohua. 2011. Dissolution of uranium-bearing minerals and mobilization of uranium by organic ligands in a biologically reduced sediment. *Environmental Science & Technology*, 45(7): 2994 ~ 2999.
- Luo Xiaozhong, Rehkämper M, Lee D C, Halliday A N. 1997. High precision $^{230}\text{Th}/^{232}\text{Th}$ and $^{234}\text{U}/^{238}\text{U}$ measurements using energy-filtered ICP magnetic sector multiple collector mass spectrometry. *International Journal of Mass Spectrometry and Ion Processes*, 171(1): 105 ~ 117.
- Luo Qukan, Cao Jian, Zhong Liang, Bai Bing, Wang Qigang, Liao Hongwei, Zong Keqing, Qin Hanlian. 2024. Research advance for uranium isotope as a quantitative proxy for paleo-oceans anoxic or oxic environment. *Caesologica Sinica*, 43(4): 957 ~ 968.
- Luo Jincheng, Shi Shaohua, Chen Youwei, Tian Jianji. 2019. Review on dating of uranium mineralization. *Acta Petrologica Sinica*, 35(2): 589 ~ 605.
- Meija J, Coplen T B, Berglund M, Brand W A, Bièvre P D, Gröning M, Holden N E, Irrgeher J, Loss R D, Walczyk T, Prohaska T. 2016. Isotopic compositions of the elements 2013 (IUPAC Technical Report). *Pure and Applied Chemistry*, 88(3): 293 ~ 306.
- Montoya-Pino C, Weyer S, Anbar A D, Pross J, Oschmann W, van de Schootbrugge B, Arz H W. 2010. Global enhancement of ocean anoxia during Oceanic Anoxic Event 2: A quantitative approach using U isotopes. *Geology*, 38(4): 315 ~ 318.
- Murphy M J, Stirling C H, Kaltenbach A, Turner S P, Schaefer B F. 2014. Fractionation of $^{238}\text{U}/^{235}\text{U}$ by reduction during low temperature uranium mineralisation processes. *Earth and Planetary Science Letters*, 388: 306 ~ 317.
- Nakanishi T, Higuchi N, Nomura M, Aida M, Fujii Y. 1996. Enrichment of U-232 by U(IV)—U(VI) Redox Ion Exchange Chromatography. *Journal of Nuclear Science and Technology* 33(4): 341 ~ 345.
- Nash J. 2010. Volcanogenic uranium deposits: Geology, geochemical processes, and criteria for resource assessment. *Open-File Report*, 2010-1001: 1 ~ 99.
- Nash J T. 2009. Recent and not-so-recent developments in uranium deposits and implications for exploration. *Economic Geology*, 104(4): 600 ~ 601.
- Nier A O. 1939. The isotopic constitution of uranium and the half-lives of the uranium isotopes. I. *Physical Review*, 55(2): 150 ~ 153.
- Nishizawa K, Nakamura K, Yamamoto T, Masuda T. 1994. Separation of strontium and barium isotopes using a crown-ether. Different behaviors of odd mass and even mass isotopes. *Solvent Extraction and Ion Exchange*, 12(5): 1073 ~ 1084.
- Nishizawa K, Satoyama T, Miki T, Yamamoto T, Hosoe M. 1995. Strontium isotope effect in liquid—liquid extraction of strontium chloride using a crown ether. *Journal of Nuclear Science and Technology*, 32(12): 1230 ~ 1235.
- Nomura M, Higuchi N, Fujii Y. 1996. Mass dependence of uranium isotope effects in the U(IV) — U(VI) exchange reaction. *Journal of the American Chemical Society*, 118(38): 9127 ~ 9130.
- Noordmann J, Weyer S, Montoya-Pino C, Dellwig O, Neubert N, Eckert S, Paetzel M, Böttcher M. E. 2015. Uranium and molybdenum isotope systematics in modern euxinic basins: Case studies from the central Baltic Sea and the Kyllaren fjord (Norway). *Chemical Geology* 396: 182 ~ 195.
- Noordmann J, Weyer S, Georg R B, Jöns S, Sharma M. 2016. $^{238}\text{U}/^{235}\text{U}$ isotope ratios of crustal material, rivers and products of hydrothermal alteration: new insights on the oceanic U isotope mass balance. *Isotopes in Environmental and Health Studies*, 52(1~2): 141 ~ 163.
- Noordmann J, Weyer S, Sharma M, Georg B, Rausch S, Bach W. 2012. Fractionation of $^{238}\text{U}/^{235}\text{U}$ during weathering and hydrothermal alteration. *Mineralogical Magazine*, 75: 1548.
- Partin C A, Bekker A, Planavsky N J, Scott C T, Gill B C, Li Chao, Podkovyrov V, Maslov A, Konhauser KO, Lalonde S V, Love G D, Poulton S W, Lyons T W. 2013. Large-scale fluctuations in Precambrian atmospheric and oceanic oxygen levels from the record of U in shales. *Earth and Planetary Science Letters*, 369~370: 284

~ 293.

- Pavia F J, Cooperdock E H G, de Obeso J C, Sims K W W, Tissot F L H, Klein F. 2023. Uranium isotopes as tracers of serpentinite weathering. *Earth and Planetary Science Letters*, 623: 118434.
- Peiffert C, Nguyen-Trung C, Cuney M. 1996. Uranium in granitic magmas; Part 2. Experimental determination of uranium solubility and fluid ~ melt partition coefficients in the uranium oxide—haplogranite—H₂O—NaX (X = Cl, F) system at 770°C, 2 kbar. *Geochimica et Cosmochimica Acta*, 60(9): 1515 ~ 1529.
- Placzek C J, Heikoop J M, House B, Linhoff B S, Pelizza M. 2016. Uranium isotope composition of waters from South Texas uranium ore deposits. *Chemical Geology*, 437: 44 ~ 55.
- Prieto C, Lozano J C, Rodríguez P B, Tomé F V. 2013. Enhancing radium solubilization in soils by citrate, EDTA, and EDDS chelating amendments. *Journal of Hazardous Materials*, 250 ~ 251: 439 ~ 446.
- Rademacher L K, Lundstrom C C, Johnson T M, Sanford R A, Zhao Juanzho, Zhang Zhaofeng. 2006. Experimentally determined uranium isotope fractionation during reduction of hexavalent U by bacteria and zero valent iron. *Environmental Science & Technology*, 40(22): 6943 ~ 6948.
- Richter S, Eykens R, Kühn H, Aregbe Y, Verbruggen A, Weyer S. 2010. New average values for the n(²³⁸U)/n(²³⁵U) isotope ratios of natural uranium standards. *International Journal of Mass Spectrometry*, 295(1): 94 ~ 97.
- Rihs S, Gaillard C, Reich T, Kohler S J. 2014. Uranyl sorption onto birnessite: A surface complexation modeling and EXAFS study. *Chemical Geology*, 373: 59 ~ 70.
- Robert T A, Lovley D R. 2002. Chapter 7 Microbial redox interactions with uranium: An environmental perspective. In: Keith —Roach M J, Livens F R. eds. *Radioactivity in the Environment*, 2: 205 ~ 223.
- Roebbert Y, Rosendahl C D, Brown A, Schippers A, Bernier-Latmani R, Weyer S. 2021. Uranium isotope fractionation during the anoxic mobilization of noncrystalline U (IV) by ligand complexation. *Environmental Science & Technology*, 55(12): 7959 ~ 7969.
- Rolison J, Stirling C, George E, Middag R, Gault-Ringold M, Rijkenberg M, de Baar H. 2015. Biogeochemical cycling of the uranium, iron and cadmium isotope systems during oceanic anoxia: A case study of the Black Sea. *Goldschmidt2015 Abstracts*; 2671.
- Rolison J M, Stirling C H, Middag R, Rijkenberg M J A. 2017. Uranium stable isotope fractionation in the Black Sea: Modern calibration of the ²³⁸U/²³⁵U paleo ~ redox proxy. *Geochimica et Cosmochimica Acta*, 203: 69 ~ 88.
- Romaniello S, Brennecke G, Anbar A, Colman A. 2009. Natural isotopic fractionation of ²³⁸U/²³⁵U in the water column of the Black Sea. *AGU Fall Meeting Abstracts*; V54C-06.
- Romaniello S J, Herrmann A D, Anbar A D. 2013. Uranium concentrations and ²³⁸U/²³⁵U isotope ratios in modern carbonates from the Bahamas: Assessing a novel paleoredox proxy. *Chemical Geology*, 362: 305 ~ 316.
- Ruzicka V. 1993. Vein uranium deposits. *Ore Geology Reviews*, 8(3): 247 ~ 276.
- Schauble E A. 2007. Role of nuclear volume in driving equilibrium stable isotope fractionation of mercury, thallium, and other very heavy elements. *Geochimica et Cosmochimica Acta*, 71(9): 2170 ~ 2189.
- Schauble E A. 2013. Modeling nuclear volume isotope effects in crystals. *Proceedings of the National Academy of Sciences*, 110(44): 17714 ~ 17719.
- Sheng Jiaru, Li Siqi, Owens J D, Wang Xiangli, Wei Yong, Ming Guodong, Huang Fang. 2024. $\delta^{238}\text{U}$ of coal reference materials determined by MC-ICP-MS. *Geostandards and Geoanalytical Research*, 48(1): 289 ~ 299.
- Sheng Jianru, Jiang Dingsheng, Erdmann S, Deng Gengxin, Duan Hhuachun, Jackson M, Devos G, Moynier F, Guo Haohu, Huang Fang. 2025a. Fluid-mediated uranium isotope fractionation in magmatic systems. *Geochemical Perspectives Letters*, 36: 1 ~ 7.
- Sheng Jiaru, Quan Yikang, Jiang Dingsheng, Deng Gengxin, Li Guangwei, Xu Zhiqin, Huang Fang. 2025b. Uranium isotope fractionation during magmatic ~ hydrothermal interactions in pegmatites. *Chemical Geology*, 677: 122632.
- Shiel A E, Johnson T M, Lundstrom C C, Laubach P G, Long P E, Williams K H. 2016. Reactive transport of uranium in a groundwater bioreduction study: Insights from high-temporal resolution ²³⁸U/²³⁵U data. *Geochimica et Cosmochimica Acta* 187: 218 ~ 236.
- Shimokawa J and Kobayash F. 1970. Separation of uranium isotopes by chemical exchange. *Isotopenpraxis Isotopes in Environmental and Health Studies*, 6(5-6): 170 ~ 176.
- Singh A, Catalano J G, Ulrich K U, Giammar D E. 2012. Molecular-scale structure of uranium (VI) immobilized with goethite and phosphate. *Environmental Science & Technology*, 46(12): 6594 ~ 6603.
- Song Jing, Tan Kaixuan, Liu Zhenzhong, Li Chunguang, Li Yongmei, Weng Zongxiang. 2022. Advances in research on uranium isotope fraction in nature and prospects. *Journal of nuclear and radiochemistry*, 44(6): 565 ~ 574.
- Spano T L, Simonetti A, Balboni E, Dorais C, Burns P C. 2017. Trace element and U isotope analysis of uraninite and ore concentrate: Applications for nuclear forensic investigations. *Applied Geochemistry*, 84: 277 ~ 285.
- Staudigel H, Plank T, White B, Schmincke H U. 1996. Geochemical fluxes during seafloor alteration of the basaltic upper oceanic crust: DSDP Sites 417 and 418. *Subduction*, 96: 19 ~ 38.
- Steiger R H and Jäger E. 1977. Subcommittee on geochronology: Convention on the use of decay constants in geo- and cosmochronology. *Earth and Planetary Science Letters*, 36(3): 359 ~ 362.
- Stirling C H, Andersen M B, Potter E K, Halliday A N. 2007. Low-temperature isotopic fractionation of uranium. *Earth and Planetary Science Letters*, 264(1): 208 ~ 225.
- Stirling C H, Andersen M B, Warthmann R, Halliday A N. 2015. Isotope fractionation of ²³⁸U and ²³⁵U during biologically-mediated uranium reduction. *Geochimica et Cosmochimica Acta*, 163: 200 ~ 218.
- Stylo M, Neubert N, Roebbert Y, Weyer S, Bernier-Latmani R. 2015a. Mechanism of uranium reduction and immobilization in desulfovibrio vulgaris biofilms. *Environmental Science & Technology*, 49(17): 10553 ~ 10561.
- Stylo M, Neubert N, Wang Y, Monga N, Romaniello S J, Weyer S, Bernier-Latmani R. 2015b. Uranium isotopes fingerprint biotic reduction. *Proceedings of the National Academy of Sciences*, 112(18): 5619 ~ 5624.
- Telus M, Dauphas N, Moynier F, Tissot FLH, Teng F Z, Nabelek P I, Craddock P R, Groat L A. 2012. Iron, zinc, magnesium and

- uranium isotopic fractionation during continental crust differentiation: The tale from migmatites, granitoids, and pegmatites. *Geochimica et Cosmochimica Acta*, 97: 247 ~ 265.
- Tissot F L H and Dauphas N. 2015. Uranium isotopic compositions of the crust and ocean: Age corrections, U budget and global extent of modern anoxia. *Geochimica et Cosmochimica Acta*, 167: 113 ~ 143.
- Tissot F L H, Dauphas N, Grove T L. 2017. Distinct $^{238}\text{U}/^{235}\text{U}$ ratios and REE patterns in plutonic and volcanic angrites: Geochronologic implications and evidence for U isotope fractionation during magmatic processes. *Geochimica et Cosmochimica Acta*, 213: 593 ~ 617.
- Tissot F L H, Ibañez ~ Mejia M. 2021. Unlocking the single-crystal record of heavy stable isotopes. *Elements*, 17(6): 389 ~ 394.
- Tissot F L H, Ibanez-Mejia M, Boehnke P, Dauphas N, McGee D, Grove T L, Harrison T M. 2019. $^{238}\text{U}/^{235}\text{U}$ measurement in single ~ zircon crystals: implications for the Hadean environment, magmatic differentiation and geochronology. *Journal of Analytical Atomic Spectrometry*, 34(10): 2035 ~ 2052.
- Uvarova Y A, Kyser T K, Geagea M L, Chipley D. 2014. Variations in the uranium isotopic compositions of uranium ores from different types of uranium deposits. *Geochimica et Cosmochimica Acta*, 146: 1 ~ 17.
- Voinot A, Kyser T K, Chipley D, Valentino M, Uvarova Y, Layton-Matthews D, Leybourne M I. 2024. Th, Mo and U isotopes in U-ore deposits record Earth's fundamental redox processes. *Chemical Geology*, 661: 1 ~ 11.
- Wang Dazhao, Leng Chengbiao, Qin Chaojian, Duan Fenghao, Zhou Wanpeng, Xu Deru. 2022. Geochemical characteristics and mineralization of uranium. *Geotectonica et Metallogenia*, 46(2): 282 ~ 302.
- Wang Xiangli, Johnson T M, Lundstrom C C. 2015. Low temperature equilibrium isotope fractionation and isotope exchange kinetics between U(IV) and U(VI). *Geochimica et Cosmochimica Acta*, 158: 262 ~ 275.
- Wang Xiangli, Planavsky N J, Reinhard C T, Hein J R, Johnson T M. 2016. A Cenozoic seawater redox record derived from $^{238}\text{U}/^{235}\text{U}$ in ferromanganese crusts. *American Journal of Science*, 316: 64 ~ 83.
- Wang Yuheng, Fruttschi M, Suvorova E, Phrommavanh V, Descostes M, Osman A A A, Geipel G, Bernier-Latmani R. 2013. Mobile uranium(IV)-bearing colloids in a mining-impacted wetland. *Nature Communications*, 4(1): 2942.
- Weyer S, Anbar A D, Gerdes A, Gordon G W, Algeo T J, Boyle E A. 2008. Natural fractionation of $^{238}\text{U}/^{235}\text{U}$. *Geochimica et Cosmochimica Acta*, 72(2): 345 ~ 359.
- Wood B J, Blundy J D, Robinson J A C. 1999. The role of clinopyroxene in generating U-series disequilibrium during mantle melting. *Geochimica et Cosmochimica Acta*, 63(10): 1613 ~ 1620.
- Yang Sha and Liu Yun. 2016. Nuclear field shift effects on stable isotope fractionation: a review. *Acta Geochimica*, 35(3): 227 ~ 239.
- Yang Sha and Liu Yun. 2015. Theoretical study of the nuclear volume effect of stable uranium isotopes. *Acta Mineralogica Sinica*, 35(S1): 1133.
- Zhang Long, Wang Fangyue, Zhou Taofa, Chen Zhenyu, Du Xiuling, Zhang Shu. 2022. The origin of uranium deposits related to the Huangmeijian A-type granite from the Lu-Zong volcanic basin, South China: Constraints from zircon U-Pb geochronology and mineral chemistry. *Ore Geology Reviews*, 141: 1 ~ 17.
- Zhang Long, Chen Zhenyu, Wang Fangyue. 2021. General characteristics and research progresses in metallogenesis of granite-related uranium deposits in South China. *Acta Petrologica Sinica*, 37(9): 2657 ~ 2676.
- Zhang Minglin, Li Shengxiang, Liu Yue, Guo Qingyin, Qin Mingkuan, Che Yongfei. 2025. Progress and prospect of global uranium exploration. *Geological Reviews*, 71(3): 1020 ~ 1028.

Advances in uranium isotope research and its applications in uranium deposits

CHAO Weiwei^{1, 2)}, YAO Dongdong²⁾, LENG Chengbiao^{1, 2)}, WANG Dazhao^{1, 2)}, WANG Yanjun^{1, 2)},
TIAN Shihong^{1, 2)}, LIANG Zhengwei^{1, 2)}, CHENG Qianglong²⁾

- 1) *National Key Laboratory of Uranium Resources Exploration—Mining and Nuclear Remote Sensing, East China University of Technology, Nanchang, 330013;*
- 2) *School of Earth and Planetary Sciences, East China University of Technology, Nanchang, 330013*

Abstract: Uranium, as a significant radioactive element in nature, demonstrates considerable scientific importance through its isotopic fractionation phenomena in studies of uranium mineralization genesis, geochemical process tracing, and environmental remediation. This contribution systematically synthesizes uranium isotope fractionation mechanisms (nuclear volume effects, redox, adsorption, and leaching processes), advanced analytical methodologies (chemical separation protocols and mass spectrometric techniques), and characteristic isotopic signatures of principal global reservoirs (continental crust, mantle, and marine systems). Furthermore, it examines applications in characterizing typical uranium deposit types, including sandstone-hosted and granite-related mineralization systems. The analysis underscores the distinctive capacity of uranium isotopes in

reconstructing metallogenic environments, tracing ore-forming material sources, and deciphering redox evolution. Prospective research directions are proposed regarding deep planetary processes, mineralization mechanisms, and mine remediation monitoring, thereby providing critical insights for advancing genetic models of uranium deposits and enhancing exploration strategies.

Keywords: uranium isotopes; isotope fractionation; nuclear volume effect; uranium deposits; redox process

Acknowledgements: This study was financially supported by the National Natural Science Foundation of China (No. 42473044), Independent Deployment Fund of the National Key Laboratory of Uranium Resources Exploration—Mining and Nuclear Remote Sensing (East China University of Technology) (No. 2025QZ-YZZ-07, 2025QZ-KF-04), Natural Science Foundation of Jiangxi Province (No. 20252BAC200255, 20252BAC220018)

First author: CHAO Weiwei, male, born in 1991, associated professor, is mainly engaged in hydrothermal deposit; Email: chaoweimei@ecut.edu.cn

Corresponding author: Leng Chengbiao, male, born in 1982, professor, is mainly engaged in teaching and research in ore deposit geology and geochemistry; Email: lcb8207@163.com

Manuscript received on: 2025-11-13; Accepted on: 2026-02-02; Published online on: 2026-02-15

Doi: 10.16509/j.georeview.2026.02.045

Edited by: ZHANG Yuxu

